ADVANCES IN GEODESY AND GEOINFORMATION
(formerly GEODESY AND CARTOGRAPHY)
Vol. 71, no. 2, article no. e23, 2022

https://doi.org/10.24425/gac.2022.141176

Original paper

The mathematical characteristic of the Laplace contour filters used in digital image processing. The third order filters

Ireneusz Winnicki*, Janusz Jasinski, Slawomir Pietrek, Krzysztof Kroszczynski

Military University of Technology, Warsaw, Poland
e-mail: ireneusz.winnicki@wat.edu.pl; ORCID: http://orcid.org/0000-0001-9170-422X
e-mail: janusz.jasinski@wat.edu.pl; ORCID: http://orcid.org/0000-0001-5634-3430
e-mail: slawomir.pietrek@wat.edu.pl; ORCID: http://orcid.org/0000-0001-9890-8487
e-mail: krzysztof.kroszczynski@wat.edu.pl; ORCID: http://orcid.org/0000-0003-1197-9915

*Corresponding author: Ireneusz Winnicki, e-mail: ireneusz.winnicki@wat.edu.pl

Received: 2022-01-10 / Accepted: 2022-04-20

Abstract: The Laplace operator is a differential operator which is used to detect edges of objects in digital images. This paper presents the properties of the most commonly used third-order 3×3 pixels Laplace contour filters including the difference schemes used to derive them. The authors focused on the mathematical properties of the Laplace filters. The basic reasons of the differences of the properties were studied and indicated using their transfer functions and modified differential equations. The relations between the transfer function for the differential Laplace operator and its difference operators were described and presented graphically. The impact of the corner elements of the masks on the results was discussed. This is a theoretical work. The basic research conducted here refers to a few practical examples which are illustrations of the derived conclusions. We are aware that unambiguous and even categorical final statements as well as indication of areas of the results application always require numerous experiments and frequent dissemination of the results. Therefore, we present only a concise procedure of determination of the mathematical properties of the Laplace contour filters matrices. In the next paper we shall present the spectral characteristic of the fifth order filters of the Laplace type.

Keywords: transfer function, finite element method, finite difference methods, matrices of the third-order Laplace filters, modified differential equations

1. Introduction

The Laplace filters matrices consideration from the point of view of numerical methods is an important aspect of the discussion presented here. Each matrix is a different difference scheme applicable to computational methods. It is a different method of solving second

order differential equation approximately in which the ∇^2 operator occurs (diffusion, waves, Laplace and other equations) – see: Richardson (1910), Shuman (1956), Ogura (1958), Miyakoda (1960), Prewitt (1970), Canny (1986), Perona (1998), Pitas (2000), Jähne (2002), Strikwerda (2004), LeVeque (2007), Burger and Burge (2008, 2009a, b, 2013), Pratt (2008), Li and Chen (2009), Mallat (2009), Lynch (2010), Parker (2011), Petrou and Petrou (2011), Gonzalez and Woods (2018). With this approach, the properties of the analyzed matrices, even seemingly alike in the process of digital images filtering, should be taken into account during solving selected issues of the mathematical physics. These properties include: consistency, convergence, order of accuracy of the finite difference equation (FDE), operators of transfer functions for each filter mask and the modified differential equation (MDE).

A modified differential equation, also called the Π-form of the first differential approximation (f.d.a.) of the scheme, is attributed to each of the discussed matrices. Using it enables to determine the order of the accuracy of the differential scheme approximating the ∇^2 operator. Furthermore, (and this is the most important issue) it unambiguously enables to determine whether a matrix is really a Laplace one. This problem is discussed in Subsection 2.3 (compare equations: (52) and (60)).

A short history of the modified differential equations and the specialist terminology used by scientists from various countries can be found in Lerat and Peyret (1973), Warming and Hyett (1974), Peyret and Taylor (1983), Li and Yang (2011), Krawczyk et al. (2012), Li and Yang (2013), Winnicki et al. (2019), Shokin et al. (2020).

This paper also explains the mathematical basics and the origin of a few practically applied Laplace filters (*masks* or *kernels*) and it draws attention to some inaccuracies (repeated in some publications) occurring in their discrete descriptions. The consequences of the inaccuracies are presented in a few selected images. The paper also indicates the elements which should compulsorily be taken into account in the procedure of linear filters matrices comparison.

Edges detection is an important issue of digital processing and analysis of images. It includes algorithms of the first level of the analysis, often called *the images initial transformation*. Valid derivation of edges, contours and vertexes simplifies location of objects (see: Marr and Hildreth, 1980; Canny, 1986; Harris and Stephens, 1988; Perona and Malik, 1990; Jähne, 1999, Jähne, 2002; Wang, 2007; Burger and Burge, 2009a,b; Krawczyk et al., 2012; Hazarika et al., 2016; Susmitha et al., 2017; Gonzalez and Woods, 2018; Reda and Kedzierski, 2020), shape recognition and distinguishing their characteristic features. In digital images the edges are created in places of large local changes of brightness between groups of pixels, i.e. in places of significant changes of orientation, reflection coefficient or lighting of objects presented in the image. The commonly applied method of determination of local discontinuities of image brightness levels and objects borders utilizes one of the variants of Laplace contour filters. At this phase, the tools of mathematical analysis are often used including research concerning function flow with respect to the function itself and its first and second derivatives in areas of large gradients of pixels brightness.

The article presents descriptions of seven selected masks of the Laplace filter used in the processing and interpretation of digital data of various origin. This may be navigation

data (Borawski, 2004; Burger and Burge, 2009a; Stateczny et al., 2020, 2021); signal processing (Mallat, 2009; Waheed et al., 2020); radar, sonar and satellite (Jasinski et al., 1999; Stateczny and Nowakowski, 2006; Kurczynski et al., 2017; Fryskowska et al., 2019; Reda and Kedzierski, 2020; Stateczny et al., 2020, 2021); geodetic and cartographic, called remote sensing in Kupidura and Kupidura (2009) and Kupidura et al. (2010); meteorological in Jasinski et al. (1999) – information about clouds including its shape, size, internal structure, as well as the relationship of the location of different types of clouds. These may also be digital images of building infrastructure elements (Burger and Burge, 2009b; Reda and Kedzierski, 2020; Wojtkowska et al., 2021) and technical devices, including military ones (Pokonieczny and Moscicka, 2018). A common goal appears in each of the listed here areas of photogrammetric research: correct edge and vertex detection of the analyzed objects.

The contextual filter is primarily a multi-element mask described by an odd order square matrix. For this reason, the final forms of most of the used Laplace filter masks together with their Π-forms of the first differential approximation are derived here.

There are a few programs used to process digital images which have embedded functions and procedures for detecting edges and contours. These include ERDAS IMAGINE and Matlab, the ones used by the authors.

The authors also want to highlight the history of the difference scheme for the differential Laplace operator starting from the late 1940s. Some of the Laplace filter masks are presented in the literature concerning the digital image processing but the names of the scientists who derived and introduced them are in general omitted.

In Section 2 we discuss the origin of some filter masks built on the basis of the finite difference method (FDM) and in Section 3 we discuss one mask built on the basis of the finite element method (FEM). In Section 4 we focused on the linear combinations of the Laplace type filter masks, including rotation of the mask. The final conclusions are presented in Section 5.

In Part II (Winnicki et al., 2022) we shall present the spectral characteristic of the fifth order filters of the Laplace type.

2. The difference Laplace filters

Laplace filter masks are induced by the two-dimensional difference operator for the partial differential equation (PDE):

$$\mathbb{A}u = \Delta u = \nabla^2 u = \frac{\partial^2 u}{\partial x^2} + \frac{\partial^2 u}{\partial y^2}, \tag{1}$$

where $u(x, y)$ is any scalar function. Assuming that the solution of (1) may be presented as an individual Fourier mode:

$$u(x_m, y_n) = u_{mn} = \hat{u} e^{i(kx_m + ly_n)}, \tag{2}$$

we obtain the transfer function for the differential Laplace equation:

$$\nabla^2 u_{mn} = -(k^2 + l^2)\hat{u} e^{i(kx_m + ly_n)} = f_L(k, l) u_{mn}, \qquad i = \sqrt{-1}, \tag{3}$$

where: $f_L(k,l) = -(k^2+l^2)$ is the transfer function for the Laplace operator (Fig. 1) and k, l – wave-numbers, $k = 2\pi/\lambda_x$, $l = 2\pi/\lambda_y$, and λ_x and λ_y – the wavelengths (compare Jähne (2002), page 329, where $f_L(\widetilde{k},\widetilde{l})$ depends on the Nyquist wave-numbers $\widetilde{k} = kh/\pi$ and $\widetilde{l} = lh/\pi$ which are the wave-numbers normalized to the maximum wave-number that can be sampled). We can also call it the transfer function of the derivative filter (see: Jähne, 2002).

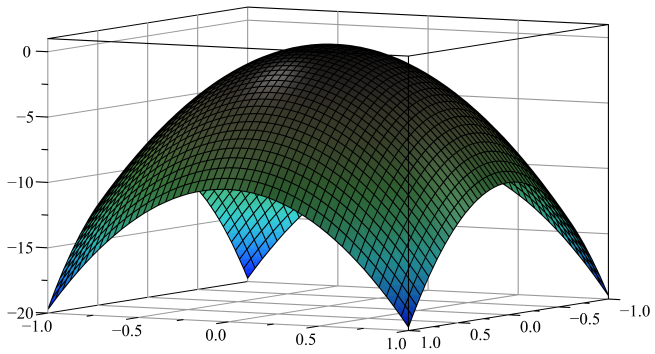

Fig. 1. The transfer function $f_L(\widetilde{k},\widetilde{l})$ for the differential Laplace equation. (The range of $(\widetilde{k},\widetilde{l})$ for all transfer functions is equal to $(\widetilde{k},\widetilde{l}) = [-1,1] \times [-1,1]$. They are symmetric)

The forms of the Laplace masks depend on the method of discretization of the differential operator (1). The methods commonly applied in practice are: the finite difference method and the finite element method (Table 1). The finite difference discretization of operator $\mathtt{A}$ (in the former method) and the approximation of the solution (in the latter) are provided on the mesh of equidistant grid nodes.

Table 1. Areas of forest cover of the Carpathian territory of Lviv region for 2016–2018

Differential Operator e.g. Laplacian ∇^2
FDM ↓ FEM
Difference Scheme
↓
Convolution Matrix (filter mask)

In the FEM the sought after solution $u(x,y)$ in $\mathtt{A}u$ is approximated by the following series:

$$u(x,y) = \sum_{i,j} u_{ij}\varphi_i(x)\psi_j(y), \tag{4}$$

where: u_{ij} – values of the function $u(x,y)$ in the grid nodes (i,j) (for example, brightness for digital images); $\varphi_i(x)$, $\psi_j(y)$ – basic functions of one variable, often called the

Lagrange elements. As it is known, both approaches presented above lead to the finite difference equations for the partial differential equations, in particular for the Laplace equation (1).

In most cases these schemes are different although they approximate the same differential operator. They differ in the forms – in the case of FEM they strictly depend on the basic functions degree and they have different characteristics. In both cases, sets of the multi-point filters in the form of 3×3 pixels matrices are obtained.

The algorithm for the filter masks construction for the differential operators of the first-, second- or higher orders is presented in Table 2. On its basis the Sobel, Prewett and, of course, Laplace filters have been derived.

The three most important features of the difference schemes which must be considered in the digital image processing are: the consistency, the order of their accuracy and the convergence. We shall discuss a few FDE derived on the basis of the Laplace discrete operator and we shall:

- check their consistency and convergence;
- estimate their order of accuracy;
- present the forms of the convolution matrices derived on the basis of these schemes;
- derive their modified differential equations which are equivalent to the Π-forms;
- present the transfer functions for the convolution operators in the analytical forms and in the forms of the Taylor series expansions with respect to the wave-numbers $(\widetilde{k}, \widetilde{l})$.

The forms of the MDEs are very useful in the detailed analysis of the dispersive and dissipative features of the difference schemes. For the elliptic partial differential equations we always obtain their Π-forms. These forms include only the space derivatives. For the partial differential equations of the hyperbolic and parabolic types at the first approach (directly after expanding the difference schemes into Taylor series) one obtains the sequence of higher order derivatives with respect to both space and time. These mixed forms are called the Γ-forms. For isolating the terms responsible for numerical dispersion and dissipation it is necessary to express all time derivatives as spatial ones (see: Appadu et al., 2008; Appadu and Dauhoo, 2011; Appadu et al., 2014; Winnicki et al., 2019; Shokin et al., 2020).

2.1. The finite difference method and the third-order Laplace filters

The discussion on the influence of the Laplace difference scheme form on the accuracy of the various numerical solutions started in the late 1940s – in the beginning of the numerical weather prediction development on the ENIAC computer by: Jule Charney, John von Neumann, Ragnar Fjørtoft and others (see: Platzman, 1979). We have to notice that the first proposal for the difference Laplace operator was presented already by Richardson (1910) – see (5). Then Hidaka (1951), scientists from the Joint Numerical Weather Prediction Unit (U.S. Air Force): Shuman (1956), Thompson (1955a,b), Knighting (1955), Ogura (1958) (Johns Hopkins University) and Miyakoda (1960) (Tokyo University) developed this issue. Their solutions – at that time applied only to the analysis of the

geostrophic vorticity and geopotential fields – are nowadays successfully used in the theory and practice of the digital images processing.

Let us focus on the difference approximations $\mathtt{A}_h u_h$ (u_h – the approximated solution) of the Laplace equation $\mathtt{A}u$. The first commonly used five-point FDE is based on the "cross" stencil (see: Richardson, 1910) and has the form:

$$\mathtt{A}_1 u_h = \frac{u_{i-1,j} + u_{i+1,j} + u_{i,j+1} + u_{i,j-1} - 4u_{i,j}}{h^2}, \tag{5}$$

where: h – spacial step of the regular square mesh, in this case – the distance between pixels (because of the convolution operation, the mesh regularity is a basic rule of constructing the masks). In presented analysis we assume that $h_x = h_y = h = 1$ in both directions of x and y. The scheme (5) leads to the following very well known filter mask:

$$\mathbf{Lap}_1 = \begin{bmatrix} 0 & 1 & 0 \\ 1 & -4 & 1 \\ 0 & 1 & 0 \end{bmatrix}. \tag{6}$$

In numerical methods, the most basic property of an applicable difference scheme is that its solutions approximate the exact solution of the partial differential equation. The difference scheme is then called convergent. The other properties which must be satisfied are: consistency and accuracy. In our further research we shall refer to the following important definitions:

Definition 1. (Strikwerda, 2004) *A finite difference equation $\mathtt{A}_h u_h$ is consistent with a partial differential equation $\mathtt{A}u$ if the difference $(\mathtt{A}_h u_h - \mathtt{A}u)$ vanishes as the sizes of the grid spacings h_x and h_y approach zero independently.*

Definition 2. (Strikwerda, 2004) *A finite difference equation $\mathtt{A}_h u_h$ is convergent if its solution $u_h(x_i, y_j)$ approaches the exact solution $u(x, y)$ of $\mathtt{A}u$ as the sizes of the grid spacings h_x and h_y approach zero.*

Definition 3. (Strikwerda, 2004) *A finite difference equation $\mathtt{A}_h u_h$ that is consistent with the partial differential equation $\mathtt{A}u$ is said to be accurate of order p and q in space if $(\mathtt{A}_h \psi - \mathtt{A}\psi) = O(h_x^p) + O(h_y^q)$ for any smooth function $\psi(x, y)$. We say that such a difference scheme's accuracy is of order (p, q).*

The MDE for (5) is presented below:

$$\Pi_1 = \nabla^2 u + \frac{h^2}{12}\left(\frac{\partial^4 u}{\partial x^4} + \frac{\partial^4 u}{\partial y^4}\right) - \frac{h^4}{360}\left(\frac{\partial^6 u}{\partial x^6} + \frac{\partial^6 u}{\partial y^6}\right) + \frac{h^6}{20160}\left(\frac{\partial^8 u}{\partial x^8} + \frac{\partial^8 u}{\partial y^8}\right) + O(h^8). \tag{7}$$

In (7) we have only the unmixed even-order partial derivatives. As $h \to 0$ the equation (7) approaches $\nabla^2 u = \dfrac{\partial^2 u}{\partial x^2} + \dfrac{\partial^2 u}{\partial y^2}$. So the FDE (5) is a consistent approximation of the Laplace equation and its solution $u_h(x_i, y_j)$ converges to the exact solution $u(x, y)$. The accuracy of the difference equation (5) is of the second order.

Applying the Euler's formula that establishes the fundamental relationship between the complex exponential function and the trigonometric functions we obtain the transfer

function for (6):

$$f_1(k,l) = -4\sin^2\frac{kh}{2} - 4\sin^2\frac{lh}{2}\,. \tag{8}$$

With the Nyquist wave-numbers introduced, the transfer function $f_L(\widetilde{k},\widetilde{l})$ takes the form: $f_L(\widetilde{k},\widetilde{l}) = -\pi^2(\widetilde{k}^2+\widetilde{l}^2)$ and the transfer function (8) takes the form:

$$f_1(\widetilde{k},\widetilde{l}) = -4\sin^2\frac{\pi\widetilde{k}}{2} - 4\sin^2\frac{\pi\widetilde{l}}{2}\,. \tag{9}$$

In the following analysis we shall apply only the Nyquist notation.

The Taylor expansion of (8) for the wave-numbers $\widetilde{k}$ and $\widetilde{l}$ up to the eighth order yields the approximation:

$$f_{1T}(\widetilde{k},\widetilde{l}) = -\pi^2\left(\widetilde{k}^2+\widetilde{l}^2\right) + \frac{\pi^4}{12}\left(\widetilde{k}^4+\widetilde{l}^4\right) - \frac{\pi^6}{260}\left(\widetilde{k}^6+\widetilde{l}^6\right) + \frac{\pi^8}{20160}\left(\widetilde{k}^6+\widetilde{l}^6\right) + O\left(\widetilde{k}^{10},\widetilde{l}^{10}\right). \tag{10}$$

Figure 2a is a graphical presentation of the transfer function (9) for the difference scheme (5) and Figure 2b for the relation $\dfrac{f_1(\widetilde{k},\widetilde{l})}{f_L(\widetilde{k},\widetilde{l})}$ (see also Fig. 12 – blue solid line).

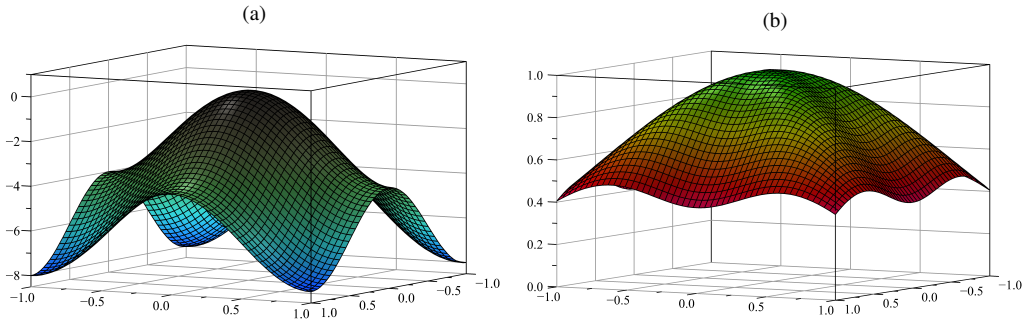

Fig. 2. The transfer function $f_1(\widetilde{k},\widetilde{l})$ for the mask (6) (a) and the graph of $\dfrac{f_1(\widetilde{k},\widetilde{l})}{f_L(\widetilde{k},\widetilde{l})}$ (b)

Knighting (1955) and Ogura (1958) proposed another difference scheme for the discretization of the Laplace operator (1):

$$\mathbb{A}_2 u_h = \frac{4(u_{i-1,j}+u_{i+1,j}+u_{i,j-1}+u_{i,j+1}) - 12u_{i,j}}{2h^2} - \frac{u_{i-1,j+1}+u_{i-1,j-1}+u_{i+1,j-1}+u_{i+1,j+1}}{2h^2}\,, \tag{11}$$

which also leads to the filter mask of the Laplace type:

$$\mathbf{Lap}_2 = \frac{1}{2}\begin{bmatrix} -1 & 4 & -1 \\ 4 & -12 & 4 \\ -1 & 4 & -1 \end{bmatrix}. \tag{12}$$

The MDE for the difference scheme (11) has the form:

$$\Pi_2 = \nabla^2 u + \frac{h^2}{12}\left(\frac{\partial^4 u}{\partial x^4} + \frac{\partial^4 u}{\partial y^4}\right) - \frac{h^4}{360}\left(\frac{\partial^6 u}{\partial x^6} + \frac{\partial^6 u}{\partial y^6}\right) + \frac{h^6}{20160}\left(\frac{\partial^8 u}{\partial x^8} + \frac{\partial^8 u}{\partial y^8}\right)$$
$$- \frac{h^2}{2}\frac{\partial^4 u}{\partial x^2 \partial y^2} + \frac{h^4}{24}\left(\frac{\partial^6 u}{\partial x^4 \partial y^2} + \frac{\partial^6 u}{\partial x^2 \partial y^4}\right) - \frac{h^6}{288}\frac{\partial^8 u}{\partial x^4 \partial y^4} + O(h^8) \tag{13}$$

and the transfer functions for (12) are as follows (see Fig. 3a):

$$f_2(\widetilde{k},\widetilde{l}) = -8\sin^2\frac{\pi\widetilde{k}}{2}\sin^2\frac{\pi\widetilde{l}}{2} - 4\sin^2\frac{\pi\widetilde{k}}{2} - 4\sin^2\frac{\pi\widetilde{l}}{2}, \tag{14}$$

$$f_{2T}(\widetilde{k},\widetilde{l}) = -\pi^2\left(\widetilde{k}^2+\widetilde{l}^2\right) + \frac{\pi^4}{12}\left(\widetilde{k}^4+\widetilde{l}^4\right) - \frac{\pi^6}{260}\left(\widetilde{k}^6+\widetilde{l}^6\right) + \frac{\pi^8}{20160}\left(\widetilde{k}^6+\widetilde{l}^6\right)$$
$$- \frac{\pi^4}{2}\widetilde{k}^2\widetilde{l}^2 + \frac{\pi^6}{24}\left(\widetilde{k}^4\widetilde{l}^2+\widetilde{k}^2\widetilde{l}^4\right) - \frac{\pi^8}{288}\widetilde{k}^4\widetilde{l}^4 + O\left(\widetilde{k}^{10},\widetilde{l}^{10}\right), \tag{15}$$

(we marked in red all the terms of the modified differential equations and transfer functions in Taylor expansion which coefficients have incorrect signs – it is, of course, the feature of the FDEs and, consequently, of the filter masks and their MDEs).

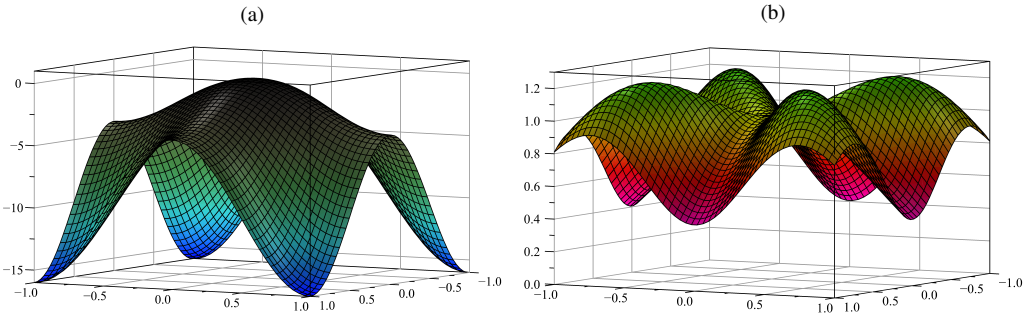

Fig. 3. The transfer function $f_2(\widetilde{k},\widetilde{l})$ for the mask (12) (a) and the graph of $\frac{f_2(\widetilde{k},\widetilde{l})}{f_L(\widetilde{k},\widetilde{l})}$ (b)

The first line of (13) is equal to the Π_1-form (7) and the first line of the expanded transfer function (15) is equal to (10) for the standard filter mask (6). The mixed partial derivatives in (13) and the products of the $\widetilde{k}$ and $\widetilde{l}$ (the second line of (15)) are the consequence of the non zero elements that appeared in the corners of matrix (12).

The sum $-\frac{h^2}{2}\frac{\partial^4 u}{\partial x^2 \partial y^2} + \frac{h^4}{24}\left(\frac{\partial^6 u}{\partial x^4 \partial y^2} + \frac{\partial^6 u}{\partial x^2 \partial y^4}\right) - \frac{h^6}{288}\frac{\partial^8 u}{\partial x^4 \partial y^4}$ in (13) describes the effects of anti-dissipation Peyret and Taylor (1983, page 51) and Winnicki et al. (2019), Shokin et al. (2020) also called backward diffusion. It follows the exponential growth of the amplitude of the elementary solution and presents the amplification features of this scheme. For medium values of the Nyquist wave-numbers the relation $\frac{f_2(\widetilde{k},\widetilde{l})}{f_L(\widetilde{k},\widetilde{l})}$ exceeds 1 – see: Figure 3b, Figure 12 – red dot-dashed line and Figure 14a. In our opinion this feature of the mask (12) introduces the noise into analyzed image which one can see on the several slanting edges in Figure 10d(3) and Figure 10d(8). Despite these features the FDE (11) is consistent and convergent as $h \to 0$ and its accuracy is of the second order.

The accuracy of the next difference scheme for the Laplace operator (1) (see: Miyakoda (1960)):

$$\mathbb{A}_3 u_h = \frac{4(u_{i-1,j} + u_{i+1,j} + u_{i,j-1} + u_{i,j+1}) - 20u_{i,j}}{2h^2} + \frac{u_{i-1,j+1} + u_{i-1,j-1} + u_{i+1,j-1} + u_{i+1,j+1}}{2h^2} \tag{16}$$

is of the fourth order (see also: LeVeque (2007), Li and Chen (2009) and Strikwerda (2004, pages 328, 331)). It leads to the forth-order filter mask of the Laplace type:

$$\mathbf{Lap}_3 = \frac{1}{6}\begin{bmatrix} 1 & 4 & 1 \\ 4 & -20 & 4 \\ 1 & 4 & 1 \end{bmatrix}. \tag{17}$$

The MDE for the difference scheme (16) has the form:

$$\Pi_3 = \nabla^2 u + \frac{1}{12}\nabla^2(\nabla^2 u) - \frac{h^4}{360}\left(\frac{\partial^6 u}{\partial x^6} + \frac{\partial^6 u}{\partial y^6}\right) + \frac{h^6}{20160}\left(\frac{\partial^8 u}{\partial x^8} + \frac{\partial^8 u}{\partial y^8}\right) - \frac{h^4}{72}\left(\frac{\partial^6 u}{\partial x^4 \partial y^2} + \frac{\partial^6 u}{\partial x^2 \partial y^4}\right) + \frac{h^6}{864}\frac{\partial^8 u}{\partial x^4 \partial y^4} + O(h^8). \tag{18}$$

In (18) we can also find the mixed even-order partial derivatives. However, the sum: $\frac{\partial^4 u}{\partial x^4} + 2\frac{\partial^4 u}{\partial^2 x \partial^2 y} + \frac{\partial^4 u}{\partial y^4}$ is equal to the bi-Laplacian which has no amplification features and the mixed derivatives of the sixth and eighth orders have only dissipative features.

The transfer function for (17) has the form (see Fig. 4a):

$$f_3(\widetilde{k},\widetilde{l}) = \frac{8}{3}\sin^2\frac{\pi\widetilde{k}}{2}\sin^2\frac{\pi\widetilde{l}}{2} - 4\sin^2\frac{\pi\widetilde{k}}{2} - 4\sin^2\frac{\pi\widetilde{l}}{2} \tag{19}$$

and its Taylor expansion contains the products of the wave-numbers $\widetilde{k}$ and $\widetilde{l}$:

$$f_{3T}(\widetilde{k},\widetilde{l}) = -\pi^2\left(\widetilde{k}^2 + \widetilde{l}^2\right) - \frac{\pi^6}{360}\left(\widetilde{k}^6 + \widetilde{l}^6\right) + \frac{\pi^8}{20160}\left(\widetilde{k}^6 + \widetilde{l}^6\right) + \frac{\pi^4}{12}\left(\widetilde{k}^4 + 2\widetilde{k}^2\widetilde{l}^2 + \widetilde{l}^4\right) - -\frac{\pi^6}{72}\left(\widetilde{k}^4\widetilde{l}^2 + \widetilde{k}^2\widetilde{l}^4\right) + \frac{\pi^8}{864}\widetilde{k}^4\widetilde{l}^4 + O\left(\widetilde{k}^{10},\widetilde{l}^{10}\right). \tag{20}$$

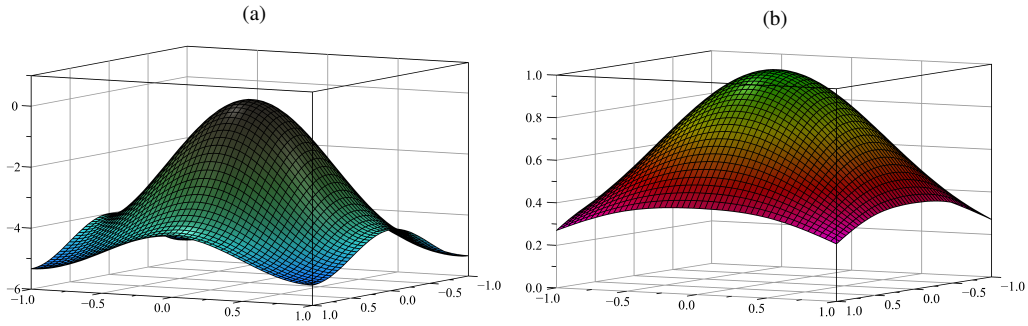

Fig. 4. The transfer function $f_3(\widetilde{k},\widetilde{l})$ for the mask (17) (a) and the graph of $\dfrac{f_3(\widetilde{k},\widetilde{l})}{f_L(\widetilde{k},\widetilde{l})}$ (b)

The first line of (20) is also the same as in the expanded transfer function (9) for the standard filter mask (6). The products of the $\widetilde{k}$ and $\widetilde{l}$ Nyquist wave-numbers (the second line of (20)) have the same origin as (15). The FDE (16) is also consistent and convergent.

The relation $\dfrac{f_3(\widetilde{k},\widetilde{l})}{f_L(\widetilde{k},\widetilde{l})}$ is presented in Figure 3b and Figure 14c.

Ogura (1958) and Thompson (1955a) derived another difference scheme of the accuracy of the second order (see also Burger and Burge (2008) and Jähne (2002, page 329) – but without the coefficient: 1/4):

$$\mathbf{Lap}_4 = \frac{1}{4}\begin{bmatrix} 1 & 2 & 1 \\ 2 & -12 & 2 \\ 1 & 2 & 1 \end{bmatrix}. \tag{21}$$

It is induced by the difference scheme of the accuracy of the second order:

$$\begin{aligned} \mathbb{A}_4 u_h = {} & \frac{2(u_{i-1,j} + u_{i+1,j} + u_{i,j-1} + u_{i,j+1}) - 12u_{i,j}}{4h^2} \\ & + \frac{u_{i-1,j+1} + u_{i-1,j-1} + u_{i+1,j-1} + u_{i+1,j+1}}{4h^2}. \end{aligned} \tag{22}$$

Its MDE is as follows:

$$\begin{aligned} \Pi_4 = {} & \nabla^2 u + \frac{h^4}{12}\left(\frac{\partial^4 u}{\partial x^4} + \frac{\partial^4 u}{\partial y^4}\right) - \frac{h^4}{360}\left(\frac{\partial^6 u}{\partial x^6} + \frac{\partial^6 u}{\partial y^6}\right) + \frac{h^6}{20160}\left(\frac{\partial^8 u}{\partial x^8} + \frac{\partial^8 u}{\partial y^8}\right) \\ & + \frac{h^2}{4}\frac{\partial^4 u}{\partial x^2 \partial y^2} - \frac{h^4}{48}\left(\frac{\partial^6 u}{\partial x^4 \partial y^2} + \frac{\partial^6 u}{\partial x^2 \partial y^4}\right) + \frac{h^6}{576}\frac{\partial^8 u}{\partial x^4 \partial y^4} + O(h^8). \end{aligned} \tag{23}$$

Both forms of the transfer functions for (21) are presented below:

$$f_4(\widetilde{k},\widetilde{l}) = 4\sin^2\frac{\pi\widetilde{k}}{2}\sin^2\frac{\pi\widetilde{l}}{2} - 4\sin^2\frac{\pi\widetilde{k}}{2} - 4\sin^2\frac{\pi\widetilde{l}}{2} \tag{24}$$

(see Fig. 5a) and

$$f_{4T}(\widetilde{k},\widetilde{l}) = -\pi^2\left(\widetilde{k}^2+\widetilde{l}^2\right) + \frac{\pi^4}{12}(\widetilde{k}^4+\widetilde{l}^4) - \frac{\pi^6}{360}\left(\widetilde{k}^6+\widetilde{l}^6\right) + \frac{\pi^8}{20160}\left(\widetilde{k}^6+\widetilde{l}^6\right) + \frac{\pi^4}{4}\widetilde{k}^2\widetilde{l}^2 - \frac{\pi^6}{48}\left(\widetilde{k}^4\widetilde{l}^2+\widetilde{k}^2\widetilde{l}^4\right) + \frac{\pi^8}{576}\widetilde{k}^4\widetilde{l}^4 + O\left(\widetilde{k}^{10},\widetilde{l}^{10}\right). \tag{25}$$

The relation $\dfrac{f_4(\widetilde{k},\widetilde{l})}{f_L(\widetilde{k},\widetilde{l})}$ is presented in Figure 5b and Figure 14d.

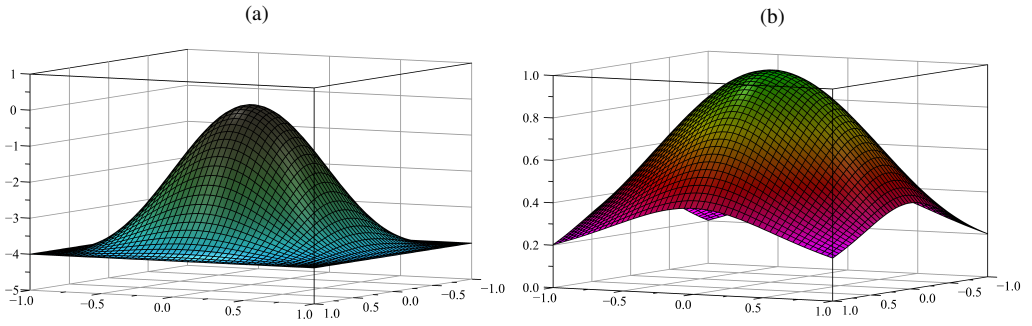

Fig. 5. The transfer function $f_4(\widetilde{k},\widetilde{l})$ for the mask (17) (a) and the graph of $\dfrac{f_4(\widetilde{k},\widetilde{l})}{f_L(\widetilde{k},\widetilde{l})}$ (b)

Jähne (2002) derived the filter mask (21) as a combination of the 1-D smoothing binomial filter $\mathbf{B}^2 = \frac{1}{4}\begin{bmatrix}1 & 2 & 1\end{bmatrix}$ and the identity matrix $\mathbf{I}$. Jähne (2002) also gave the form of the transfer function (page 554):

$$f_{4J}(\widetilde{k},\widetilde{l}) = 4\cos^2\frac{\pi\widetilde{k}}{2}\cos^2\frac{\pi\widetilde{l}}{2} - 4. \tag{26}$$

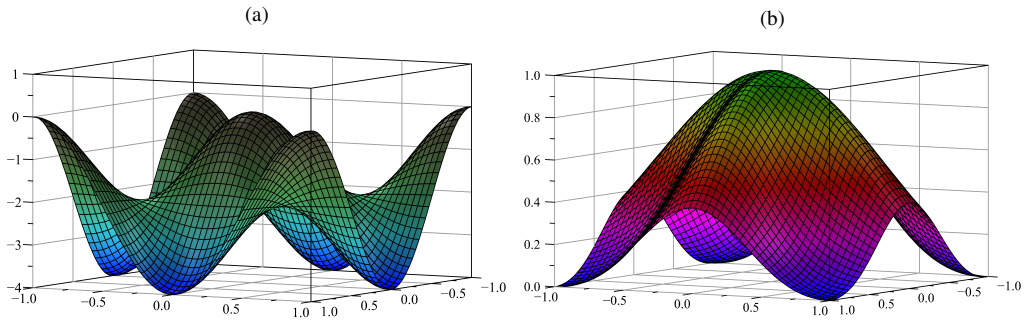

Fig. 6. The transfer function $f_5(\widetilde{k},\widetilde{l})$ for the mask (27) (a) and the graph of $\dfrac{f_5(\widetilde{k},\widetilde{l})}{f_L(\widetilde{k},\widetilde{l})}$ (b)

Of course, the transfer function (24) is equivalent to (26). The difference scheme (22) is consistent and convergent.

The following five-point "diagonal" or "square" stencil is an alternative to the filter mask (6) based on the "cross" stencil:

$$\mathbf{Lap}_5 = \frac{1}{2}\begin{bmatrix} \boxed{1} & 0 & \boxed{1} \\ 0 & -4 & 0 \\ \boxed{1} & 0 & \boxed{1} \end{bmatrix} = \frac{1}{2}\begin{bmatrix} 0 & 1 & 0 \\ 1 & -4 & 1 \\ 0 & 1 & 0 \end{bmatrix}^{\measuredangle 45^\circ}. \tag{27}$$

The mask (27) is obtained by rotating the mask (6) by 45° to the left or to the right. It is used in numerical weather prediction in the analysis of the semi-geostrophic adaptation process. It is derived on the basis of the FDE:

$$\mathbb{A}_5 u_h = \frac{u_{i-1,j-1} + u_{i+1,j-1} + u_{i-1,j+1} + u_{i+1,j+1} - 4u_{i,j}}{(\sqrt{2}h)^2}. \tag{28}$$

Its MDE is as follows:

$$\Pi_5 = \nabla^2 u + \frac{h^4}{12}\left(\frac{\partial^4 u}{\partial x^4} + \frac{\partial^4 u}{\partial y^4}\right) - \frac{h^4}{360}\left(\frac{\partial^6 u}{\partial x^6} + \frac{\partial^6 u}{\partial y^6}\right) + \frac{h^6}{20160}\left(\frac{\partial^8 u}{\partial x^8} + \frac{\partial^8 u}{\partial y^8}\right)$$
$$+ \frac{h^2}{2}\frac{\partial^4 u}{\partial x^2 \partial y^2} - \frac{h^4}{24}\left(\frac{\partial^6 u}{\partial x^4 \partial y^2} + \frac{\partial^6 u}{\partial x^2 \partial y^4}\right) + \frac{h^6}{288}\frac{\partial^8 u}{\partial x^4 \partial y^4} + O(h^8). \tag{29}$$

The forms of the transfer functions for (27) are presented below (see also Fig. 5a):

$$f_5(\widetilde{k},\widetilde{l}) = 8\sin^2\frac{\pi\widetilde{k}}{2}\sin^2\frac{\pi\widetilde{l}}{2} - 4\sin^2\frac{\pi\widetilde{k}}{2} - 4\sin^2\frac{\pi\widetilde{l}}{2}, \tag{30}$$

$$f_{5T}(\widetilde{k},\widetilde{l}) = -\pi^2\left(\widetilde{k}^2 + \widetilde{l}^2\right) + \frac{\pi^4}{12}\left(\widetilde{k}^4 + \widetilde{l}^4\right) - \frac{\pi^6}{360}\left(\widetilde{k}^6 + \widetilde{l}^6\right) + \frac{\pi^8}{20160}\left(\widetilde{k}^6 + \widetilde{l}^6\right)$$
$$+ \frac{\pi^4}{2}\widetilde{k}^2\widetilde{l}^2 - \frac{\pi^6}{24}\left(\widetilde{k}^4\widetilde{l}^2 + \widetilde{k}^2\widetilde{l}^4\right) + \frac{\pi^8}{288}\widetilde{k}^4\widetilde{l}^4 + O(\widetilde{k}^{10},\widetilde{l}^{10}). \tag{31}$$

The sum underlined in (31) is opposite to the sum underlined in (15). The FDE (28) is consistent and convergent. Its order of accuracy is 2. Let us note that for large Nyquist wave-numbers the relation of $\dfrac{f_5(\widetilde{k},\widetilde{l})}{f_L(\widetilde{k},\widetilde{l})}$ is equal to zero (see Fig. 5b and Fig. 12 – dark green solid line and Fig. 14e).

3. The FEM and the third-order Laplace filters

In another method of constructing the difference schemes for the partial differential equations, called the Galerkin method, we approximate the sought after solution $u(x, y)$ instead of the differential operator $\mathbb{A}$. Its particular case is the finite element method.

Let us consider the Poisson equation in the fixed domain Ω:

$$\mathbb{A}u = \Delta u = -\sum_{k=1}^{2} \frac{\partial^2 u}{\partial x_k^2} = f(x_1, x_2), \tag{32}$$

where: $x_1 = x$ and $x_2 = y$; $u(x, y)$, $f(x, y)$ are given functions on $\Omega = \mathbb{R} \times \mathbb{R} = [0, 1] \times [0, 1]$ domain. If $f(x, y) = 0$, equation (32) becomes the Laplace equation. In our problem the boundary conditions for (32) are unimportant (see: Strang and Fix (2008), Le Dret and Lucquin (2016) and below).

According to the finite element method technique one can assume that on a fixed domain Ω the solution $u^h(x, y)$ of (32) may be written as the series:

$$u^h(x, y) = \sum_{i=1}^{M} \sum_{j=1}^{N} u_{i,j} \theta_{i,j}(x, y) = \sum_{i=1}^{M} \sum_{j=1}^{N} u_{i,j} \varphi_i(x) \psi_j(y), \tag{33}$$

where: $\theta_{i,j}(x, y) = \varphi_i(x)\psi_j(y)$ – the bilinear function with separated variables. The coefficients $u_{i,j}$ are the primary unknowns once the basis has been selected. The basis functions $\varphi_i(x)$ and $\psi_j(x)$ are called the shape or trial functions. They can be linear, quadratic or cubic functions. It is important to notice that the compact support of each shape function is *small*, i.e. it is given by a few elements.

In 2-dimensional cases the variational formulation of (32) for the solution $u(x, y) \in H_0^1$ (H_0^1 – Sobolev space) leads for $\forall \xi(x, y) \in H_0^1$ to the equation:

$$\int_{\Omega} \mathbb{A}u\xi \, \mathrm{d}\Omega = -\int_{\Omega} \Delta u \xi \, \mathrm{d}\Omega = \int_{\Omega} f\xi \, \mathrm{d}\Omega, \tag{34}$$

where: $\xi(x, y)$ – so called test function. Applying the Green formula for integrating by parts to (34) we obtain:

$$\int_{\Omega} \sum_{i=1}^{2} D_i u D_i \xi \, \mathrm{d}\Omega - \int_{\partial\Omega} \frac{\partial u}{\partial n} \xi \, \mathrm{d}\Gamma = \int_{\Omega} f\xi \, \mathrm{d}\Omega, \tag{35}$$

where: $D_1 = \dfrac{\partial}{\partial x}$, $D_2 = \dfrac{\partial}{\partial y}$ and $\dfrac{\partial u}{\partial n} = \nabla u \cdot \mathbf{n} = \displaystyle\sum_{i=1}^{2} \frac{\partial u}{\partial x_i} n_i$ denotes the normal derivative of u on $\partial\Omega$.

The expression:

$$a(u, \xi) = \int_{\Omega} \sum_{i=1}^{2} D_i u D_i \xi \, \mathrm{d}\Omega, \tag{36}$$

is called the bilinear form on $H_0^1 \times H_0^1$ and $a(.,.)$ is an inner product. The bilinear form (36) leads to the discrete approximation for the Laplace operator.

In linear cases, the shape functions $\varphi_i(x)$ and $\psi_j(x)$ are called *chapeau functions* or *hat functions* and they have the forms of the Lagrange linear polynomials:

$$\varphi_i(x) = \begin{cases} \dfrac{x - x_{i-1}}{h}, & x_{i-1} \le x \le x_i \\ \dfrac{x_{i+1} - x}{h}, & x_i \le x \le x_{i+1} \\ 0 & \text{otherwise} \end{cases}, \quad \psi_j(x) = \begin{cases} \dfrac{y - y_{j-1}}{h}, & y_{j-1} \le y \le y_j \\ \dfrac{y_{j+1} - y}{h}, & y_j \le y \le y_{j+1} \\ 0 & \text{otherwise} \end{cases}. \tag{37}$$

The equations (37) describe the piecewise linear approximating functions with small support. It means that the functions vanish outside some compact subset of Ω – see Figure 7.

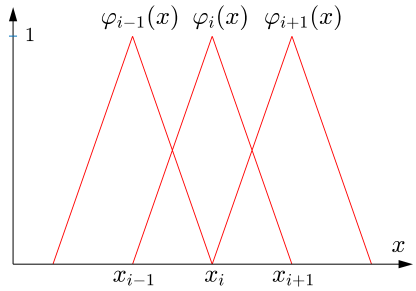

Fig. 7. The *hat functions* with support $[x_{i-1}, x_{i+1}]$

Let us assume that the test functions $\{\xi_{i,j}(x, y)\}$ also have separated variables and, similarly to trial functions, they have compact support on Ω. It means that these functions are bounded on Ω and vanish outside it. If we additionally accept that $\xi_{i,j}(x, y) = \varphi_i(x)\psi_j(y)$ then $\{\theta_{i,j}(x, y)\} = \{\xi_{i,j}(x, y)\}$ – the trial functions and the test functions are equal. The choice of $\{\theta_{i,j}(x, y)\}$ and $\{\xi_{i,j}(x, y)\}$ with compact support leads to the finite element methods (it is the fundamental assumption of the FEM; see: Lynch (2010) and Strang and Fix (2008)).

We can now pose the problem to find in 2-dimensional space of functions $u^h \in S_h$ such one that:

$$a(u^h, \theta) = (f, \theta), \quad \forall \theta \in S_h\,, \quad S_h \subset H_0^1\,. \tag{38}$$

The interpolation error of our problem is defined below.

Theorem 1. *Let $u^h(x, y)$ and $u(x, y)$ be the solutions of (38) and (36). Then*

$$\left\| u^h - u \right\| \le Ch^2 \|u\|_2, \tag{39}$$

where: C– positive constant.

If we introduce the partitions of the domain $\Omega = [0, 1] \times [0, 1]$:

$$\begin{aligned} 0 = x_0 < \cdots x_{i-1} < x_i < x_{i+1} < \cdots < x_M = 1, \\ 0 = y_0 < \cdots y_{j-1} < y_j < y_{j+1} < \cdots < y_N = 1, \end{aligned} \tag{40}$$

then the projection of (35) on subset $[x_{i-1}, x_{i+1}] \times [y_{j-1}, y_{j+1}]$ of Ω takes the form (for $f(x,y) = 0$):

$$\begin{aligned}\iint_{\Omega} (u_{xx} + u_{yy})\xi(x,y)\,\mathrm{d}x\,\mathrm{d}y &= -\iint_{\Omega} \left(\frac{\partial u}{\partial x}\frac{\partial \xi}{\partial x} + \frac{\partial u}{\partial y}\frac{\partial \xi}{\partial y}\right)\mathrm{d}x\,\mathrm{d}y \\ &= -\iint_{\Omega} \sum_{i=1}^{M}\sum_{j=1}^{N} u_{i,j}\frac{\partial \theta_{i,j}}{\partial x}\frac{\partial \xi_{k,l}}{\partial x}\,\mathrm{d}x\,\mathrm{d}y - \iint_{\Omega} \sum_{i=1}^{M}\sum_{j=1}^{N} u_{i,j}\frac{\partial \theta_{i,j}}{\partial y}\frac{\partial \xi_{k,l}}{\partial y}\,\mathrm{d}x\,\mathrm{d}y \\ &= -\sum_{i=1}^{M}\sum_{j=1}^{N} u_{i,j}\iint_{\Omega}\left(\frac{\partial \theta_{i,j}}{\partial x}\frac{\partial \xi_{k,l}}{\partial x} + \frac{\partial \theta_{i,j}}{\partial y}\frac{\partial \xi_{k,l}}{\partial y}\right)\mathrm{d}x\,\mathrm{d}y = -\sum_{i=1}^{M}\sum_{j=1}^{N} u_{i,j}K_{i,j}\,, \end{aligned} \tag{41}$$

where:

$$\mathbf{K} = -\int_{x_{i-1}}^{x_{i+1}}\int_{y_{j-1}}^{y_{j+1}}\left(\frac{\partial \theta_{i,j}}{\partial x}\frac{\partial \xi_{k,l}}{\partial x} + \frac{\partial \theta_{i,j}}{\partial y}\frac{\partial \xi_{k,l}}{\partial y}\right)\mathrm{d}x\,\mathrm{d}y \quad \begin{matrix} 0 < i, & k < M \\ 0 < j, & l < N \end{matrix}\,, \tag{42}$$

is known as the stiffness matrix.

The boundary conditions:

$$\int_{\partial\Omega} \frac{\partial u^h}{\partial n}\xi(x,y)\,\mathrm{d}s = \int_{y_{j-1}}^{y_{j+1}} \xi(x,y)\,\frac{\partial u^h}{\partial x}\bigg|_{x_{i-1}}^{x_{i+1}}\mathrm{d}y + \int_{x_{i-1}}^{x_{i+1}} \xi(x,y)\,\frac{\partial u^h}{\partial y}\bigg|_{y_{j-1}}^{y_{j+1}}\mathrm{d}x \tag{43}$$

are omitted because for every i and j the function $\xi_{i,j}(x,y)$ vanishes at the endpoints of the subset of Ω (see: (37)). Let us derive a few elements of matrix $\mathbf{K}$. For example, $K_{i-1,j-1}$ has the value:

$$\begin{aligned} K_{i-1,j-1} &= -\int_{x_{i-1}}^{x_{i+1}}\int_{y_{j-1}}^{y_{j+1}}\left(\overbrace{\frac{\partial \varphi_{i-1}}{\partial x}\psi_{j-1}}^{\frac{\partial \theta_{i-1j-1}}{\partial x}}\overbrace{\frac{\partial \varphi_i}{\partial x}\psi_j}^{\frac{\partial \xi_{ij}}{\partial x}} + \overbrace{\frac{\partial \psi_{j-1}}{\partial y}\varphi_{i-1}}^{\frac{\partial \theta_{i-1j-1}}{\partial y}}\overbrace{\frac{\partial \psi_j}{\partial y}\varphi_i}^{\frac{\partial \xi_{ij}}{\partial y}}\right)\mathrm{d}x\,\mathrm{d}y \\ &= -\frac{1}{h^3}\int_{y_{j-1}}^{y_j}(y_j - y)(y - y_{j-1})\,\mathrm{d}y - \frac{1}{h^3}\int_{x_{i-1}}^{x_i}(x_i - x)(x - x_{i-1})\,\mathrm{d}x = \frac{1}{3}\,. \end{aligned} \tag{44}$$

The elements of $\mathbf{K}$ in the remaining corners have the same value. We obtain similar values for the nodes on the cross (for: $(i\pm1, j)$ and $(i, j\pm1)$. For $i = j$ the central element $K_{i,j}$ is equal to (we integrate only over a closed interval $[y_{j-1}, y_j]$ because of the symmetry):

$$K_{ij} = -4\int_{y_{j-1}}^{y_j}\left(\int_{x_{i-1}}^{x_i}\frac{\partial \varphi_i}{\partial x}\frac{\partial \varphi_i}{\partial x}\,\mathrm{d}x + \int_{x_i}^{x_{i+1}}\frac{\partial \varphi_i}{\partial x}\frac{\partial \varphi_i}{\partial x}\,\mathrm{d}x\right)\psi_j\psi_j\,\mathrm{d}y = -\frac{8}{3}\,. \tag{45}$$

As the result we obtain the difference scheme built on the basis of the FEM with linear Lagrange polynomials:

$$\mathbb{A}_6 u_h = \frac{u_{i-1,j} + u_{i+1,j} + u_{i,j-1} + u_{i,j+1} - 8u_{i,j}}{3h^2} + \frac{u_{i-1,j+1} + u_{i-1,j-1} + u_{i+1,j-1} + u_{i+1,j+1}}{3h^2} \tag{46}$$

and 3×3 pixels mask of the contour Laplace filter:

$$\mathbf{K} = \mathbf{Lap}_6 = \frac{1}{3}\begin{bmatrix} 1 & 1 & 1 \\ 1 & -8 & 1 \\ 1 & 1 & 1 \end{bmatrix}. \tag{47}$$

The mask (47) is also presented e.g. in Burger and Burge (2008, page 132), Lynch (2010, page 234), Gonzalezand Woods (2018, page 161). Pratt (2007) and Prewitt (1970) present this filter with incorrect coefficient equal to $-1/8$. None of the mentioned authors published its derivation.

The MDE for (46) is given below:

$$\Pi_6 = \nabla^2 u + \frac{h^4}{12}\left(\frac{\partial^4 u}{\partial x^4} + \frac{\partial^4 u}{\partial y^4}\right) - \frac{h^4}{360}\left(\frac{\partial^6 u}{\partial x^6} + \frac{\partial^6 u}{\partial y^6}\right) + \frac{h^6}{20160}\left(\frac{\partial^8 u}{\partial x^8} + \frac{\partial^8 u}{\partial y^8}\right) + \frac{h^2}{3}\frac{\partial^4 u}{\partial x^2 \partial y^2} - \frac{h^4}{36}\left(\frac{\partial^6 u}{\partial x^4 \partial y^2} + \frac{\partial^6 u}{\partial x^2 \partial y^4}\right) + \frac{h^6}{432}\frac{\partial^8 u}{\partial x^4 \partial y^4} + O(h^8). \tag{48}$$

The transfer function for (47) has the form (see Fig. 8a):

$$f_6(\widetilde{k}, \widetilde{l}) = \frac{16}{3}\sin^2\frac{\pi\widetilde{k}}{2}\sin^2\frac{\pi\widetilde{l}}{2} - 4\sin^2\frac{\pi\widetilde{k}}{2} - 4\sin^2\frac{\pi\widetilde{l}}{2}. \tag{49}$$

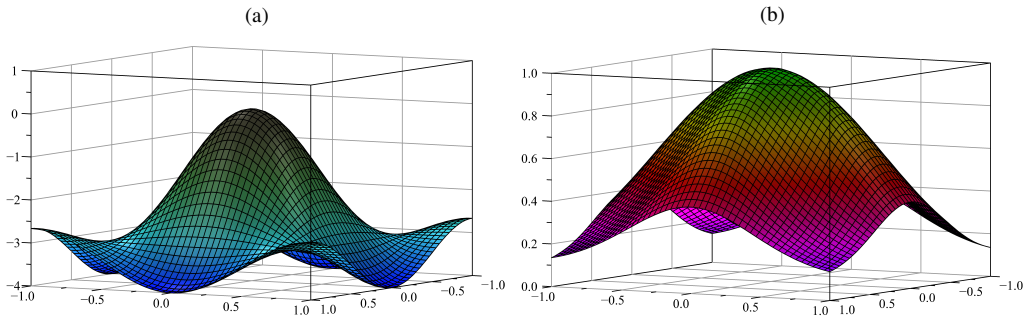

Fig. 8. The transfer function $f_6(\widetilde{k}, \widetilde{l})$ for the mask (47) (a) and the graph of $\dfrac{f_6(\widetilde{k}, \widetilde{l})}{f_L(\widetilde{k}, \widetilde{l})}$ (b)

It is similar to the classical *Mexican hat* filter. Its Taylor expansion also contains the products of the wave-numbers $\widetilde{k}$ and $\widetilde{l}$:

$$f_{6T}(\widetilde{k},\widetilde{l}) = -\pi^2\left(\widetilde{k}^2+\widetilde{l}^2\right) + \frac{\pi^4}{12}\left(\widetilde{k}^4+\widetilde{l}^4\right) - \frac{\pi^6}{360}\left(\widetilde{k}^6+\widetilde{l}^6\right) + \frac{\pi^8}{20160}\left(\widetilde{k}^6+\widetilde{l}^6\right) + \frac{\pi^4}{3}\widetilde{k}^2\widetilde{l}^2 - \frac{\pi^6}{36}\left(\widetilde{k}^4\widetilde{l}^2+\widetilde{k}^2\widetilde{l}^4\right) + \frac{\pi^8}{432}\widetilde{k}^4\widetilde{l}^4 + O\left(\widetilde{k}^{10},\widetilde{l}^{10}\right). \tag{50}$$

The relation $\dfrac{f_6(\widetilde{k},\widetilde{l})}{f_L(\widetilde{k},\widetilde{l})}$ is presented in Figure 8b and Figure 14f. See also Figure 12 – magenta solid line.

The difference scheme (46) is consistent and convergent and its accuracy is of the second order (see Theorem 1).

4. The linear combinations of the Laplace type filter masks

Some authors (see for example: Pratt (2007, page 503), Prewitt (1970, page 126) and Borawski (2004), Tadeusiewicz and Korohoda (1997)) present another filter mask:

$$\mathbf{FM} = \begin{bmatrix} 1 & -2 & 1 \\ -2 & 4 & -2 \\ 1 & -2 & 1 \end{bmatrix} \tag{51}$$

and they state that it is also a filter mask of the Laplace type (Pratt (2007) and Prewitt (1970) present it with a coefficient equal to $1/4$). However, after detailed analysis it occurs that this mask does not induce any Laplace difference operator despite its symmetry and the sum of all elements (51) being equal to zero, so typical for it. The origin of this mask is quite interesting. Repeating the transformation presented above we come to the conclusion that the mask (51) is induced by the mixed fourth-order derivatives – one of the terms of the biharmonic equation:

$$\Pi_{\mathbf{FM}} = h^4\frac{\partial^4 u}{\partial x^2\partial y^2} + O(h^6) \tag{52}$$

and not by the standard Laplace differential operator:

$$\mathbb{A}u = \frac{\partial^2 u}{\partial x^2} + \frac{\partial^2 u}{\partial y^2}.$$

The equivalent of the transfer function is presented below:

$$f_{\mathbf{FM}}(\widetilde{k},\widetilde{l}) = 16\sin^2\frac{\pi\widetilde{k}}{2}\sin^2\frac{\pi\widetilde{l}}{2}. \tag{53}$$

Both graphs in Figure 9a and Figure 9b confirm that the mask (51) is the best for corners detection. Let us also notice that the filter mask (51) can also be obtained by the following subtraction:

$$\frac{3}{2}\left(\mathbf{Lap}_3 - \mathbf{Lap}_2\right) = \frac{1}{4}\begin{bmatrix}1 & 4 & 1\\ 4 & -20 & 4\\ 1 & 4 & 1\end{bmatrix} - \frac{3}{4}\begin{bmatrix}-1 & 4 & -1\\ 4 & -12 & 4\\ -1 & 4 & -1\end{bmatrix} = \begin{bmatrix}1 & -2 & 1\\ -2 & 4 & -2\\ 1 & -2 & 1\end{bmatrix}. \tag{54}$$

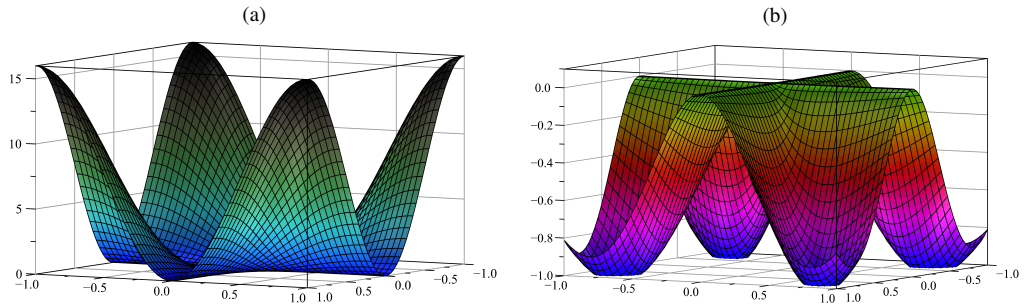

Fig. 9. The transfer function $f_{\mathbf{FM}}(\widetilde{k},\widetilde{l})$ for the mask (51) (a) and the graph of $\dfrac{f_{\mathbf{FM}}(\widetilde{k},\widetilde{l})}{f_L(\widetilde{k},\widetilde{l})}$ (b)

The FDE for the right-hand side of (54) has the form:

$$\frac{4u_{i,j} - 2(u_{i-1,j} + u_{i+1,j} + u_{i,j-1} + u_{i,j+1})}{h^2} + \frac{u_{i-1,j+1} + u_{i-1,j-1} + u_{i+1,j-1} + u_{i+1,j+1}}{h^2} = O(h^4). \tag{55}$$

The mask (51) is also the result of the product of the 1-D second-order Laplace difference filters:

$$\begin{bmatrix}1\\ -2\\ 1\end{bmatrix}\begin{bmatrix}1 & -2 & 1\end{bmatrix} = \begin{bmatrix}1 & -2 & 1\\ -2 & 4 & -2\\ 1 & -2 & 1\end{bmatrix}. \tag{56}$$

The mask (51) could be an alternative to the Harris corner detector method for digital image processing applied to figures with horizontal and vertical edges (see: Burger and Burge (2008) and Harris and Stephens (1988)). A few plane figures: square, triangle, pentagon, parallelogram, star, square with rounded corners (squircle), cross and rhombus are presented in Figure 10a. The same plane figures after filtering by means of the mask (51) are presented in Figure 10b.

The main premise of the Harris corner detector is that the corner points exist where the gradient of the image, described by any function $I(x, y)$, is strong at least in two directions. In general, the directions do not have to be perpendicular. To locate these strong gradients Harris and Stephens (1988) proposed to compute the first partial derivatives of the image function: $\dfrac{\partial I}{\partial x}$ and $\dfrac{\partial I}{\partial y}$. The process of automatic corners detecting is nontrivial, therefore

the Harris procedure is rather complicated. It is precisely described in Burger and Burge (2008) (see also the Java source code there).

Note that in Figure 10b all horizontal and vertical edges were removed from the figures by the mask (51): all edges in the square (Fig. 10b(1)), the bases of the triangle (Fig. 10b(2)), pentagon (Fig. 10b(3)) and parallelogram (Fig. 10b(4)), here also the upper edge). The mask (51) also removed wide fragments of the horizontal and vertical edges of the squircle (Fig. 10b(6)). The star (Fig. 10b(5)) and the rhombus (Fig. 10b(8)) are not changed because their edges are neither horizontal nor vertical.

The most interesting plane figure is the cross (Fig. 10b(7)) where filtering its image reduced all perpendicular (horizontal and vertical) line-like structures to the corner pixels.

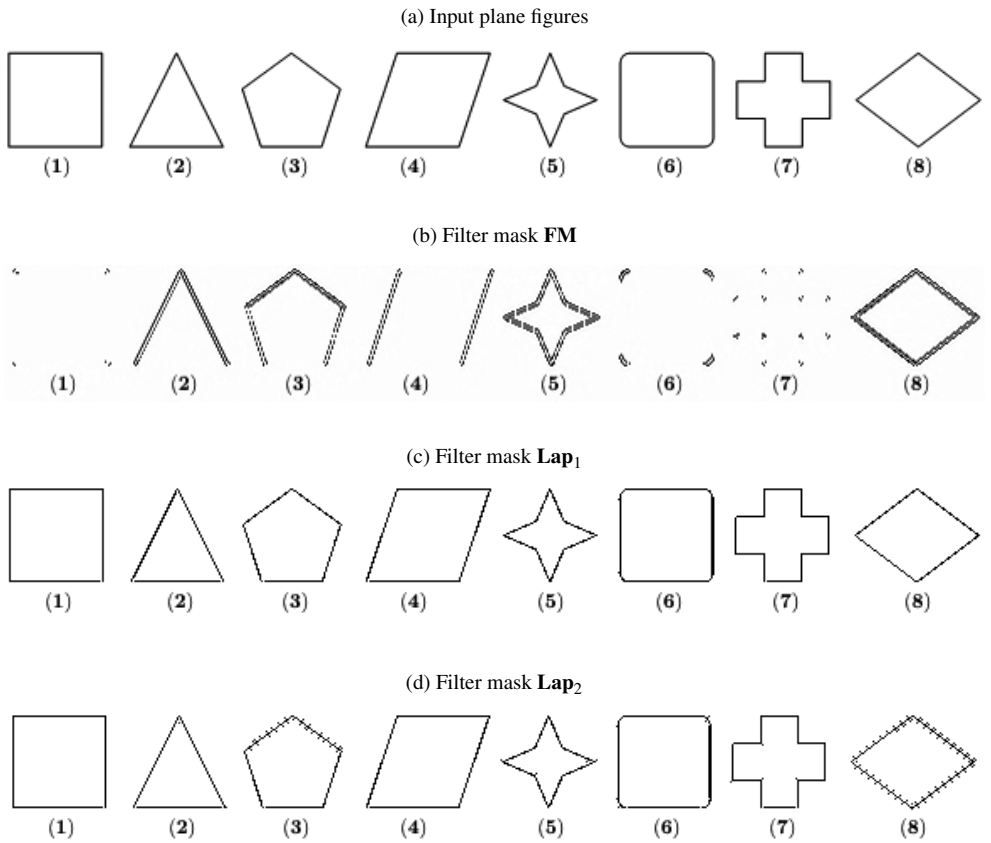

Fig. 10. The differences in filtering of the plane geometrical figures (a) by means of the masks: (51) (b); (6) (c) and (12) (d)

In our analysis we come to the conclusion that the filter mask **FM** described by (51) is not isotropic (see: Perona and Malik (1990), Scharr (2000), Scharr and Weickert (2000)). The isotropic mask is described in Kamgar-Parsi et al. (1999) and the multiscale edge detection in lapped transform domain in Hazarika et al. (2016). It strongly depends on

the edges orientation. If the edges are neither horizontal nor vertical the filter mask (51) is "blind" to the edges (see for example the triangle, pentagon, parallelogram, star and rhombus). Therefore, the mask (51) must not be called a filter mask of the Laplace type (the Laplace kernels highlight the edges). As it was already earlier mentioned, the mask (12) introduces noise into the analyzed image which one can see on the several slanting edges in Figure 10d3 and Figure 10d(8). The filter mask (6) introduces no noise (Fig. 10c).

Let us carry out a numerical test. Fig. 11a presents a field of any function $I(x, y)$ determined by the script *peaks.m* in which one can appoint strong gradient, weak gradient and gradient-less areas of the function $I(x, y)$. Let us filter this field by the oldest Laplace mask $\mathbf{Lap}_1$ (Fig. 11b) and then by the mask **FM** (Fig. 11c). The natural feature of the filter masks of the Laplace type is that they generally highlight regions of rapid changes of the function $I(x, y)$ values. The gradients of these changes are clearly seen as the isolines of the vertical projections of the tested and filtered fields of *peaks.m* on the horizontal plane in Figure 11a and Figure 11b. The Laplace filters sharpen the gradients

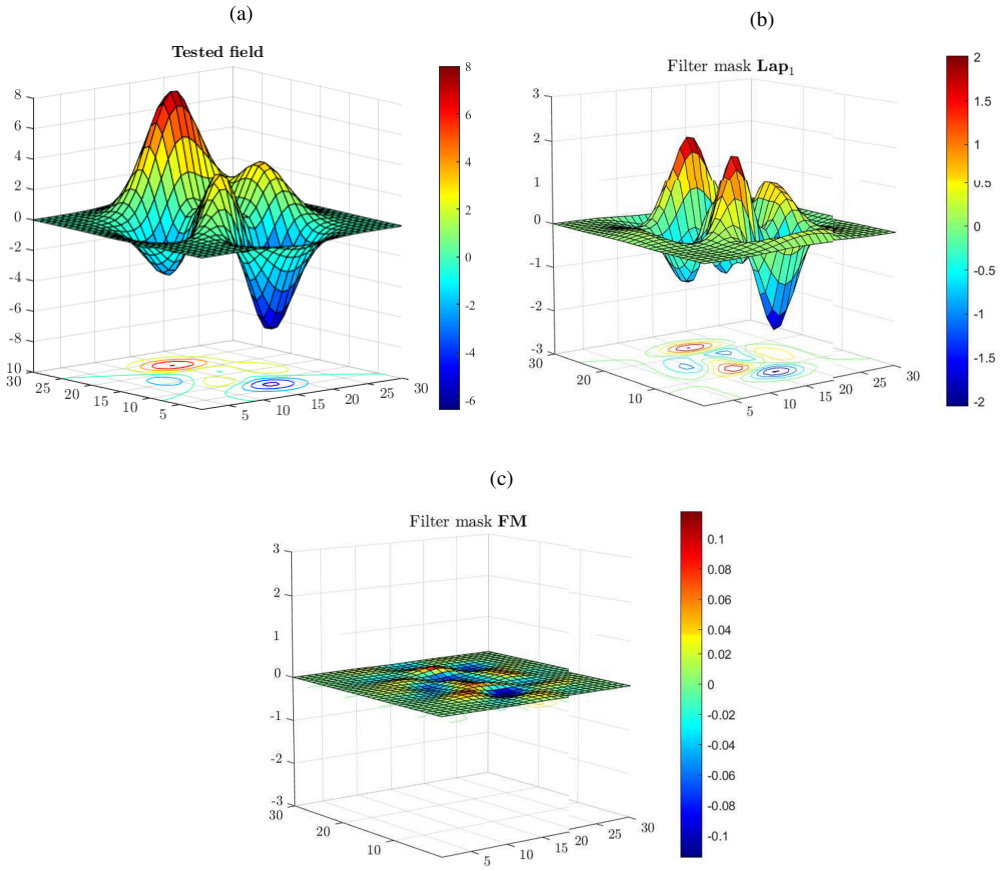

Fig. 11. Tested field (a), the tested field after filtering by means of the mask (6) (b) and the tested field after filtering by means of the mask (51) (c)

but, unfortunately, they usually reduce the maxima and the minima of the magnitudes of any fluctuation (compare the ranges of the color bars in Fig. 11a and Fig. 11b). In general, the shape of the tested field is conserved.

Let us also note that the filter mask (51) cut all the fluctuations in the analyzed fields (Fig. 11c). The equivalent $f_{\mathbf{FM}}(\widetilde{k},\widetilde{l})$ (53) of the transfer function is equal 0 in the range of $(\widetilde{k},\widetilde{l}) = [-0.9, 0.9] \times [-0.9, 0.9]$ (see Fig. 9a). The magnitude of the remaining fluctuations is less than $|0.12|$ while the maximum of the magnitude of the test field in Figure 11a is approximately equal to $|8.12|$. So, in our opinion the presented example is the best proof that the mask (51) is not of the Laplace type. The sum of all elements of this filter is equal to zero, however, it is the feature of all kernels applied to corners detection.

Table 2. Masks of the third-order filters and their first differential approximations (f.d.a.)

Masks	The shortened-forms of the the f.d.a – MDE: $\overline{\nabla^2 u}^0 = \frac{h^2}{12}\left(\frac{\partial^4 u}{\partial x^4}+\frac{\partial^4 u}{\partial y^4}\right) - \frac{h^4}{360}\left(\frac{\partial^6 u}{\partial x^6}+\frac{\partial^6 u}{\partial y^6}\right) + \frac{h^6}{20160}\left(\frac{\partial^8 u}{\partial x^8}+\frac{\partial^8 u}{\partial y^8}\right)$
$\begin{bmatrix} 0 & 1 & 0 \\ 1 & -4 & 1 \\ 0 & 1 & 0 \end{bmatrix}$	$\overline{\nabla^2 u}^1 = \nabla^2 u + \overline{\nabla^2 u}^0 + O(h^8)$
$\frac{1}{2}\begin{bmatrix} -1 & 4 & -1 \\ 4 & -12 & 4 \\ -1 & 4 & -1 \end{bmatrix}$	$\overline{\nabla^2 u}^2 = \nabla^2 u + \overline{\nabla^2 u}^0 - \frac{h^2}{2}\frac{\partial^4 u}{\partial x^2 \partial y^2} + \frac{h^4}{24}\left(\frac{\partial^6 u}{\partial x^4 \partial y^2}+\frac{\partial^6 u}{\partial x^2 \partial y^4}\right) - \frac{h^6}{288}\frac{\partial^8 u}{\partial x^4 \partial y^4} + O(h^8)$
$\frac{1}{6}\begin{bmatrix} 1 & 4 & 1 \\ 4 & -20 & 4 \\ 1 & 4 & 1 \end{bmatrix}$	$\overline{\nabla^2 u}^3 = \nabla^2 u + \overline{\nabla^2 u}^0 + \frac{1}{12}\nabla^2(\nabla^2 u) - \frac{h^4}{360}\left(\frac{\partial^6 u}{\partial x^6}+\frac{\partial^6 u}{\partial y^6}\right) + \frac{h^6}{20160}\left(\frac{\partial^8 u}{\partial x^8}+\frac{\partial^8 u}{\partial y^8}\right) - \frac{h^4}{72}\left(\frac{\partial^6 u}{\partial x^4 \partial y^2}+\frac{\partial^6 u}{\partial x^2 \partial y^4}\right) + \frac{h^6}{864}\frac{\partial^8 u}{\partial x^4 \partial y^4} + O(h^8)$
$\frac{1}{4}\begin{bmatrix} 1 & 2 & 1 \\ 2 & -12 & 2 \\ 1 & 2 & 1 \end{bmatrix}$	$\overline{\nabla^2 u}^4 = \nabla^2 u + \overline{\nabla^2 u}^0 + \frac{h^2}{4}\frac{\partial^4 u}{\partial x^2 \partial y^2} - \frac{h^4}{48}\left(\frac{\partial^6 u}{\partial x^4 \partial y^2}+\frac{\partial^6 u}{\partial x^2 \partial y^4}\right) + \frac{h^6}{576}\frac{\partial^8 u}{\partial x^4 \partial y^4} + O(h^8)$
$\frac{1}{2}\begin{bmatrix} 1 & 0 & 1 \\ 0 & -4 & 0 \\ 1 & 0 & 1 \end{bmatrix}$	$\overline{\nabla^2 u}^5 = \nabla^2 u + \overline{\nabla^2 u}^0 + \frac{h^2}{2}\frac{\partial^4 u}{\partial x^2 \partial y^2} - -\frac{h^4}{24}\left(\frac{\partial^6 u}{\partial x^4 \partial y^2}+\frac{\partial^6 u}{\partial x^2 \partial y^4}\right) + \frac{h^6}{288}\frac{\partial^8 u}{\partial x^4 \partial y^4} + O(h^8)$
$\frac{1}{3}\begin{bmatrix} 1 & 1 & 1 \\ 1 & -8 & 1 \\ 1 & 1 & 1 \end{bmatrix}$	$\overline{\nabla^2 u}^6 = \nabla^2 u + \overline{\nabla^2 u}^0 + \frac{h^2}{3}\frac{\partial^4 u}{\partial x^2 \partial y^2} - \frac{h^4}{36}\left(\frac{\partial^6 u}{\partial x^4 \partial y^2}+\frac{\partial^6 u}{\partial x^2 \partial y^4}\right) + \frac{h^6}{432}\frac{\partial^8 u}{\partial x^4 \partial y^4} + O(h^8)$
$\frac{1}{3}\begin{bmatrix} -2 & 1 & -2 \\ 1 & 4 & 1 \\ -2 & 1 & -2 \end{bmatrix}$	$\overline{\nabla^2 u}^7 = \nabla^2 u + \overline{\nabla^2 u}^0 + \frac{2h^2}{3}\frac{\partial^4 u}{\partial x^2 \partial y^2} - \frac{h^4}{18}\left(\frac{\partial^6 u}{\partial x^4 \partial y^2}+\frac{\partial^6 u}{\partial x^2 \partial y^4}\right) + \frac{h^6}{216}\frac{\partial^8 u}{\partial x^4 \partial y^4} + O(h^8)$

Table 3. Transfer functions in Taylor series expansions

Operators	Transfer functions: $f_0(\widetilde{k},\widetilde{l}) = -\pi^2\left(\widetilde{k}^2+\widetilde{l}^2\right)+\frac{\pi^4}{12}\left(\widetilde{k}^4+\widetilde{l}^4\right)-\frac{\pi^6}{360}\left(\widetilde{k}^6+\widetilde{l}^6\right)+\frac{\pi^8}{20160}\left(\widetilde{k}^6+\widetilde{l}^6\right)$
$\frac{\partial^2 u}{\partial x^2}+\frac{\partial^2 u}{\partial y^2}$	$f_L = -\pi^2\left(\widetilde{k}^2+\widetilde{l}^2\right)$
$\begin{bmatrix}0&1&0\\1&-4&1\\0&1&0\end{bmatrix}$	$f_{1T}(\widetilde{k},\widetilde{l}) = f_0(\widetilde{k},\widetilde{l})+O\left(\widetilde{k}^{10},\widetilde{l}^{10}\right)$
$\frac{1}{2}\begin{bmatrix}-1&4&-1\\4&-12&4\\-1&4&-1\end{bmatrix}$	$f_{2T}(\widetilde{k},\widetilde{l}) = f_0(\widetilde{k},\widetilde{l})-\frac{\pi^4}{2}\widetilde{k}^2\widetilde{l}^2+\frac{\pi^6}{24}\left(\widetilde{k}^4\widetilde{l}^2+\widetilde{k}^2\widetilde{l}^4\right)-\frac{\pi^8}{288}\widetilde{k}^4\widetilde{l}^4+O\left(\widetilde{k}^{10},\widetilde{l}^{10}\right)$
$\frac{1}{6}\begin{bmatrix}1&4&1\\4&-20&4\\1&4&1\end{bmatrix}$	$f_{3T}(\widetilde{k},\widetilde{l}) = f_0(\widetilde{k},\widetilde{l})+\frac{\pi^4}{6}\widetilde{k}^2\widetilde{l}^2-\frac{\pi^6}{72}\left(\widetilde{k}^4\widetilde{l}^2+\widetilde{k}^2\widetilde{l}^4\right)+\frac{\pi^8}{864}\widetilde{k}^4\widetilde{l}^4+O\left(\widetilde{k}^{10},\widetilde{l}^{10}\right)$
$\frac{1}{4}\begin{bmatrix}1&2&1\\2&-12&2\\1&2&1\end{bmatrix}$	$f_{4T}(\widetilde{k},\widetilde{l}) = f_0(\widetilde{k},\widetilde{l})+\frac{\pi^4}{4}\widetilde{k}^2\widetilde{l}^2-\frac{\pi^6}{48}\left(\widetilde{k}^4\widetilde{l}^2+\widetilde{k}^2\widetilde{l}^4\right)+\frac{\pi^8}{576}\widetilde{k}^4\widetilde{l}^4+O\left(\widetilde{k}^{10},\widetilde{l}^{10}\right)$
$\frac{1}{2}\begin{bmatrix}1&0&1\\0&-4&0\\1&0&1\end{bmatrix}$	$f_{5T}(\widetilde{k},\widetilde{l}) = f_0(\widetilde{k},\widetilde{l})+\frac{\pi^4}{2}\widetilde{k}^2\widetilde{l}^2-\frac{\pi^6}{24}\left(\widetilde{k}^4\widetilde{l}^2+\widetilde{k}^2\widetilde{l}^4\right)+\frac{\pi^8}{288}\widetilde{k}^4\widetilde{l}^4+O\left(\widetilde{k}^{10},\widetilde{l}^{10}\right)$
$\frac{1}{3}\begin{bmatrix}1&1&1\\1&-8&1\\1&1&1\end{bmatrix}$	$f_{6T}(\widetilde{k},\widetilde{l}) = f_0(\widetilde{k},\widetilde{l})+\frac{\pi^4}{3}\widetilde{k}^2\widetilde{l}^2-\frac{\pi^6}{36}\left(\widetilde{k}^4\widetilde{l}^2+\widetilde{k}^2\widetilde{l}^4\right)+\frac{\pi^8}{432}\widetilde{k}^4\widetilde{l}^4+O\left(\widetilde{k}^{10},\widetilde{l}^{10}\right)$
$\frac{1}{3}\begin{bmatrix}-2&1&-2\\1&4&1\\-2&1&-2\end{bmatrix}$	$f_{7T}(\widetilde{k},\widetilde{l}) = f_0(\widetilde{k},\widetilde{l})+\frac{2\pi^4}{3}\widetilde{k}^2\widetilde{l}^2-\frac{\pi^6}{18}\left(\widetilde{k}^4\widetilde{l}^2+\widetilde{k}^2\widetilde{l}^4\right)+\frac{\pi^8}{216}\widetilde{k}^4\widetilde{l}^4+O\left(\widetilde{k}^{10},\widetilde{l}^{10}\right)$

4.1. The rotation of the filter masks

Let us apply the very popular proceedings in the digital images processing – the rotation of the filter mask (see also: Scharrand and Weickert (2000), Weickert and Scharr (2002)) – and let us rotate the mask (56) by 45° (the same result is both for counterclockwise and clockwise rotation).

$$\begin{bmatrix}-2&1&-2\\1&4&1\\-2&1&-2\end{bmatrix}\xleftarrow[\measuredangle 45^\circ]{}\begin{bmatrix}1&-2&1\\-2&-4&-2\\1&-2&1\end{bmatrix}\xrightarrow[\measuredangle -45^\circ]{}\begin{bmatrix}-2&1&-2\\1&4&1\\-2&1&-2\end{bmatrix}. \tag{57}$$

This yields the following mask:

$$\widetilde{\mathbf{FM}}_{\pm 45^\circ} = \begin{bmatrix} -2 & 1 & -2 \\ 1 & 4 & 1 \\ -2 & 1 & -2 \end{bmatrix}, \tag{58}$$

for which the transfer function has the form:

$$f_{\widetilde{\mathbf{FM}}_{\pm 45^\circ}}(\widetilde{k}, \widetilde{l}) = -32 \sin^2 \frac{\pi \widetilde{k}}{2} \sin^2 \frac{\pi \widetilde{l}}{2} + 12 \sin^2 \frac{\pi \widetilde{k}}{2} + 12 \sin^2 \frac{\pi \widetilde{l}}{2}. \tag{59}$$

Expanding (58) into its $\Pi-$form (the difference scheme is at this stage omitted) one obtains the shortened incorrect MDE:

$$\Pi_{\text{incor}} = -3\left(\frac{\partial^2 u}{\partial x^2} + \frac{\partial^2 u}{\partial y^2}\right) - \frac{h^2}{4}\left(\frac{\partial^4 u}{\partial x^4} + \frac{\partial^4 u}{\partial y^4}\right) - 2h^2 \frac{\partial^4 u}{\partial x^2 \partial y^2}. \tag{60}$$

It means that the correct kernel form for the filter which should be equivalent of the Laplace difference operator should be equal to:

$$\mathbf{Lap}_7 = -\frac{1}{3}\widetilde{\mathbf{FM}}_{\pm 45^\circ} = -\frac{1}{3}\begin{bmatrix} -2 & 1 & -2 \\ 1 & 4 & 1 \\ -2 & 1 & -2 \end{bmatrix} = \frac{1}{3}\begin{bmatrix} 2 & -1 & 2 \\ -1 & -4 & -1 \\ 2 & -1 & 2 \end{bmatrix}. \tag{61}$$

The filter mask $\mathbf{Lap}_7$ of the Laplace type is another proposal for the digital image processing. Its derivation on the basis of the modified differential equation has not been published so far. Pratt (2007) analyzed this mask with the coefficient: $-1/8$.

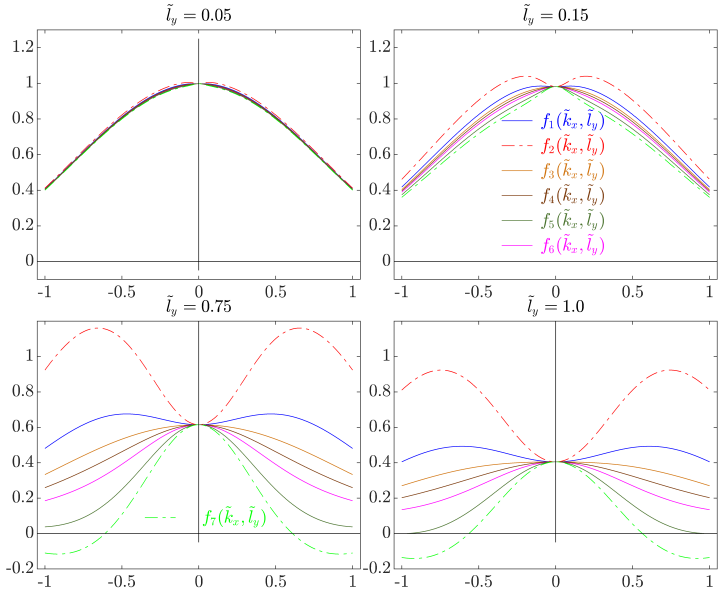

Fig. 12. The graphs of the functions $\dfrac{f_p(\widetilde{k}, \widetilde{l} = \text{const})}{f_L(\widetilde{k}, \widetilde{l} = \text{const})}$ for $\widetilde{l} = 0.05, \widetilde{l} = 0.15, \widetilde{l} = 0.75, \widetilde{l} = 1.0$, $p = 1 \pm 7$

Below we present the transfer function $f_7(\widetilde{k},\widetilde{l})$ (Fig. 13), the FDE for the right-hand side of (61) and the correct form of the modified differential equation $\mathbf{\Pi}_7$ for the mask (61):

$$f_7(\widetilde{k},\widetilde{l}) = \frac{32}{3}\sin^2\frac{\pi\widetilde{k}}{2}\sin^2\frac{\pi\widetilde{l}}{2} - 4\sin^2\frac{\pi\widetilde{k}}{2} - 4\sin^2\frac{\pi\widetilde{l}}{2}, \tag{62}$$

$$f_{7T}(\widetilde{k},\widetilde{l}) = -\pi^2\left(\widetilde{k}^2+\widetilde{l}^2\right) + \frac{\pi^4}{12}(\widetilde{k}^4+\widetilde{l}^4) - \frac{\pi^6}{360}\left(\widetilde{k}^6+\widetilde{l}^6\right) + \frac{\pi^8}{20160}\left(\widetilde{k}^6+\widetilde{l}^6\right) + \frac{2\pi^4}{3}\widetilde{k}^2\widetilde{l}^2 - \frac{\pi^6}{18}(\widetilde{k}^4\widetilde{l}^2+\widetilde{k}^2\widetilde{l}^4) + \frac{\pi^8}{216}\widetilde{k}^4\widetilde{l}^4 + O\left(\widetilde{k}^{10},\widetilde{l}^{10}\right), \tag{63}$$

– the finite difference equation:

$$\mathbb{A}_7 u = \frac{2(u_{i-1,j+1}+u_{i-1,j-1}+u_{i+1,j-1}+u_{i+1,j+1})}{3h^2} - \frac{u_{i-1,j}+u_{i+1,j}+u_{i,j-1}+u_{i,j+1}+4u_{i,j}}{3h^2}, \tag{64}$$

– the correct form of the modified differential equation:

$$\Pi_7 = \nabla^2 u + \frac{h^4}{12}\left(\frac{\partial^4 u}{\partial x^4}+\frac{\partial^4 u}{\partial y^4}\right) - \frac{h^4}{360}\left(\frac{\partial^6 u}{\partial x^6}+\frac{\partial^6 u}{\partial y^6}\right) + \frac{h^6}{20160}\left(\frac{\partial^8 u}{\partial x^8}+\frac{\partial^8 u}{\partial y^8}\right) + \frac{2h^2}{3}\frac{\partial^4 u}{\partial x^2\partial y^2} - \frac{h^4}{18}\left(\frac{\partial^6 u}{\partial x^4\partial y^2}+\frac{\partial^6 u}{\partial x^2\partial y^4}\right) + \frac{h^6}{216}\frac{\partial^8 u}{\partial x^4\partial y^4} + O(h^8). \tag{65}$$

The difference scheme (65) is consistent and convergent and its accuracy is of the second order.

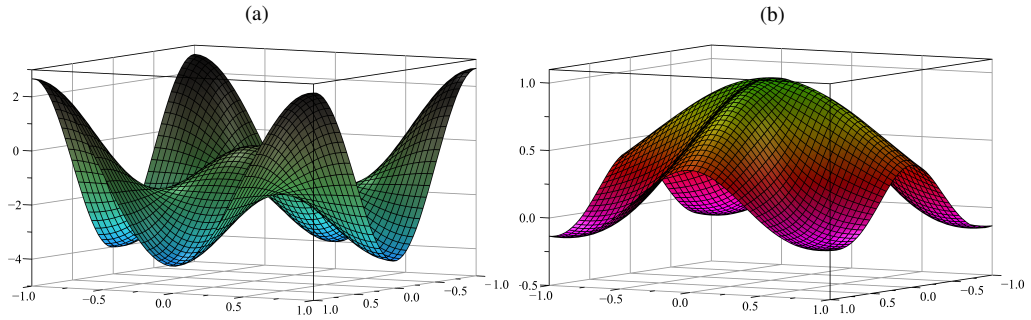

Fig. 13. The transfer function $f_7(\widetilde{k},\widetilde{l})$ for the mask (61) (a) and the graph of $\dfrac{f_7(\widetilde{k},\widetilde{l})}{f_L(\widetilde{k},\widetilde{l})}$ (b)

5. The final conclusions

We discussed the features of seven filter masks of the third order for the Laplace differential operator $\mathbb{A}u = \dfrac{\partial^2 u}{\partial x^2} + \dfrac{\partial^2 u}{\partial y^2}$. Six of them were derived on the basis of the finite difference method and one on the basis of the finite element method with approximation of the solution $u(x, y)$ by means of bi-linear Lagrange elements. The MDEs and the transfer functions for each of them were also presented here (see: Table 2 and Table 3). We also discussed the features of the mask (51) which is not induced by the Laplace operator.

Conclusions

1. All the presented masks satisfy the standard condition and the necessary condition for the Laplace difference operator: the sums of all elements of the filter masks $\mathbf{Lap}_1 \div \mathbf{Lap}_7$ and also of the **FM** mask are equal to zero (see Jähne et al. (1999)). We also observe that halves of the sums of the absolute values of all elements of the masks: $\mathbf{Lap}_1$ and $\mathbf{Lap}_3 \div \mathbf{Lap}_7$ are equal to the absolute values of their central elements: $\dfrac{1}{2} \sum\limits_{\substack{i=1\div 3 \\ j=1\div 3}} |a_{i,j}| = |a_{2,2}|$. It is not the necessary condition (see below) but it can be treated as the sufficient condition. We can also find that for the mask $\mathbf{Lap}_2$ half of this sum is equal to 16 and it is much greater than $|a_{2,2}|$ (see: (12)). This last observation is confirmed by the graphs of the transfer function $f_2(\widetilde{k}, \widetilde{l})$ – see Figure 12 (red dot-dashed line) and (13) or (15) (see also Fig. 14a). It could mean that application of the Knighting (1955) and Ogura (1958) proposition to the medium values of $(\widetilde{k}, \widetilde{l})$ is rather limited.
2. The coefficients in the truncation error $-\dfrac{h^4}{72}\left(\dfrac{\partial^6 u}{\partial x^4 \partial y^2} + \dfrac{\partial^6 u}{\partial x^2 \partial y^4}\right) + \dfrac{h^6}{864}\dfrac{\partial^8 u}{\partial x^4 \partial y^4}$ of the MDE (18) (see mask (17)) are the smallest (see: Table 2). It could lead to the statement that this filter mask of the accuracy of the fourth order is the best. Unfortunately, the graphs of the function $f_3(\widetilde{k}, \widetilde{l})$ (Fig. 12 – brown solid line and Fig. 14b) do not confirm it. In the set of the filters of the third order the spectral features of the Laplace filter mask (17) are not the best in the range of $(\widetilde{k}, \widetilde{l}) = [-1, 1] \times [-1, 1]$. They are worse in comparison with the transfer function $f_1(\widetilde{k}, \widetilde{l})$. However, from the other point of view, the transfer function $f_3(\widetilde{k}, \widetilde{l})$ is characterized by the highest regularity as a function of the Nyquist wave-numbers, especially for $(\widetilde{k}, \widetilde{l}) \to \pm 1$ (smooth graph, one maximum, no minimum and inflection points).
3. Continuing this discussion one should notice that the term $-4\sin^2\dfrac{\pi\widetilde{k}}{2} - 4\sin^2\dfrac{\pi\widetilde{l}}{2}$ Richardson (1910) mask appears in all expressions which describe the transfer functions for the filter masks of the Laplace type: $\mathbf{Lap}_1 \div \mathbf{Lap}_7$. So, one can assume

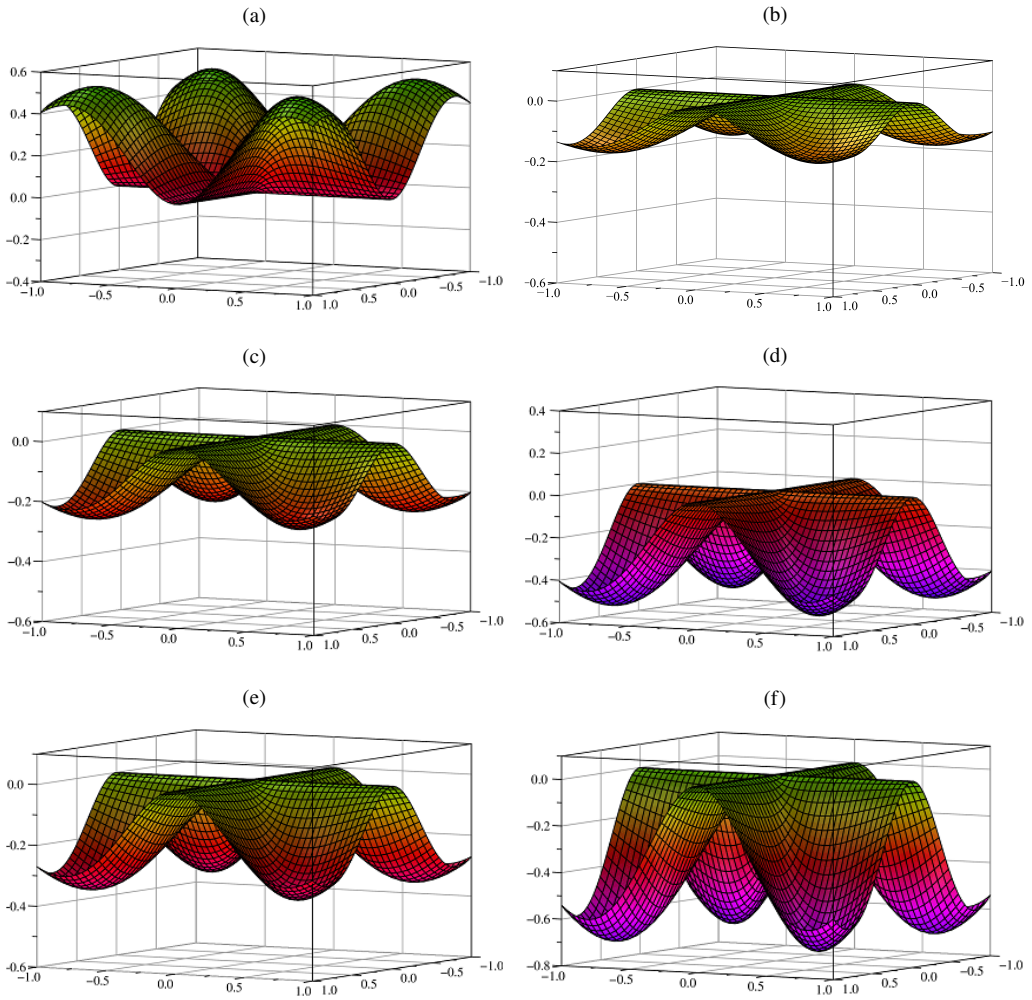

Fig. 14. The influence of the filter masks corner elements $\dfrac{f_p(\widetilde{k},\widetilde{l}) - f_1(\widetilde{k},\widetilde{l})}{f_L(\widetilde{k},\widetilde{l})}$ $(p = 2 \div 7)$ on the conformity of their transfer functions to the transfer function $f_L(\widetilde{k},\widetilde{l})$ for: $f_2(\widetilde{k},\widetilde{l})$ (a), $f_3(\widetilde{k},\widetilde{l})$ (b), $f_4(\widetilde{k},\widetilde{l})$ (c), $f_5(\widetilde{k},\widetilde{l})$ (d), $f_6(\widetilde{k},\widetilde{l})$ (e) and $f_7(\widetilde{k},\widetilde{l})$ (f)

that the remaining terms in the transfer functions for $\mathbf{Lap}_2 \div \mathbf{Lap}_7$ come from the corner elements of the matrices. The graphs of the influence of the corner elements on their conformity to the exact function:

$$\frac{f_p(\widetilde{k},\widetilde{l}) - f_1(\widetilde{k},\widetilde{l})}{f_L(\widetilde{k},\widetilde{l})} \quad (p = 2 \div 7) \tag{66}$$

are presented in Figure 14. The important role of the corner elements in the transfer functions features is double adverse with respect to the standard mask (6). If they are

negative, the values of (66) are positive and the transfer function (14) (Knighting (1955) and Ogura (1958)) amplifies certain features of the Laplace filter mask (see: $\mathbf{Lap}_2$). In the opposite case, if the corner elements are positive, the values of (66) are negative and the other masks have strongly dissipative features. It can be interpreted as numerical diffusion that damps the other features of the filter masks. The influence of the corner elements on the results is the smallest for the filter masks of the accuracy of the fourth order (see Fig. 14b).

4. We also come to the conclusion that the filter mask **FM** (51) is not isotropic. It strongly depends on the edges orientation. If the edges are neither horizontal nor vertical the filter mask (51) is "blind" – it does not introduce any changes (see for example the triangle in Fig. 10b2).
5. In many monographs and papers examples may be found that for data that are neither smooth nor continuous the finite element method is much better than the finite difference method. We cannot confirm it in this paper. The coefficients in the transfer function (50) for $\mathbf{Lap}_6$ and at the mixed derivatives in the modified differential equation (48) are greater than these in $\mathbf{Lap}_3$ or $\mathbf{Lap}_4$. It means that the spectral characteristics of the mask $\mathbf{Lap}_6$ are worse.

The final difference approximations and the Taylor series expansions of the transfer functions for the analyzed filter masks of the Laplace type are collected in Table 2 and Table 3.

Finally, analyzing Figure 14 we come to the conclusion that the spectral features of the Knighting (1955) and Ogura (1958) mask (12) is the worst (graph (a)). In numerical methods, a difference scheme characterized by backward diffusion is said to be an anti-dissipative one and, in general, it amplifies non-physical solutions (see: Winnicki et al. (2019)). Figure 3b, Figure 12 (red dot-dashed line) and Figure 14a confirm this observation.

Author contributions

Conceptualization: I.W.; methodology: S.P. and K.K.; validation: J.J. and K.K.; writing original draft preparation: I.W.; writing – review and editing: J.J; supervision: I.W.; project administration: I.W.; funding acquisition: J.J.

Data availability statement

No datasets were used in this research.

Acknowledgements

The research was funded by the Military University of Technology, Faculty of Civil Engineering and Geodesy within the grant number 531-4000-22-871/UGB/2021.

References

Appadu, A.R., Dauhoo, M.Z., Rughooputh, S.D. D.V. (2008). Control of numerical effects of dispersion and dissipation in numerical schemes for efficient shock-capturing through an optimal Courant number. *Comput. Fluids*, 37(6), 767–783. DOI: 10.1016/j.compfluid.2007.07.018.

Appadu, A.R., and Dauhoo, M.Z. (2011). The Concept of Minimized Integrated Exponential Error for Low Dispersion and Low Dissipation Schemes. *Int. J. Numerical Methods Fluids*, 65(5), 578–601. DOI: 10.1002/fld.2206.

Appadu, A.R. (2014). Optimized Low Dispersion and Low Dissipation Runge-Kutta Algorithms in Computational Aeroacoustics. *Appl. Math. Inf. Sci.*, 8(1), 57–68. DOI: 10.12785/amis/080106.

Borawski, M. (2004). *Preliminary digital image processing*. In: Methods of Comparative Navigation (in Polish), 88–119. Gdynia: Andrzej Stateczny GTN.

Burger, W., and Burge, M.J. (2008). *Digital Image Processing. An Algorithmic Introduction Using Java. Texts in Computer Science*. New York: Springer Science + Business Media.

Burger, W., and Burge, M.J. (2009a). Principles of Digital Image Processing. Core Algorithms. London: Springer – Verlag.

Burger, W., and Burge, M.J. (2009b). Principles of Digital Image Processing. Fundamental Techniques. London: Springer – Verlag.

Burger, W., and Burge, M.J. (2013). Principles of Digital Image Processing. Advanced Methods. London: Springer – Verlag.

Canny, J.F. (1986). A computational approach to edge detection. *IEEE Trans. Pattern Anal. Mach. Intell.*, 8(6), 679–695. DOI: 10.1109/TPAMI.1986.4767851.

Fryskowska, A., Kedzierski, M., Wierzbicki, D. et al. (2019). Analysis of imagery interpretability of open sources radar satellite imagery. In: Proceedings of 12th Conference on Reconnaissance and Electronic Warfare Systems (CREWS). Oltarzew (2019). DOI: 10.1117/12.2525013.

Gonzalez, R.C., and Woods, R.E. (2018). *Digital Image Processing, 4 edn. Pearson International Edition*. New Jersey: Pearson Education.

Harris, C., and Stephens, M. (1988). *A combined corner and edge detector*. In Taylor C.J. (Eds.) Proceedings of the Alvey Vision Conference, p. 23.1–23.6. DOI: 10.5244/C.2.23.

Hazarika, D., Nath, V.K., and Bhuyan, M. (2016). SAR Image Despeckling Based on Combination of Laplace Mixture Distribution with Local Parameters and Multiscale Edge Detection in Lapped Transform Domain. *Procedia Comput. Sci.*, 87, 140–147. DOI: 10.1016/j.procs.2016.05.140.

Hidaka, K. (1951). Stencils for integrating partial differential equations of mathematical physics. *Sci. Math. Jpn.*, 11(1).

Jähne, B., Scharr, H., Körkel, S. et al. (1999). *Principles of filter design*. In: Handbook of computer vision and applications, 2, 125–151. Academic Press.

Jähne, B. (2002). Digital Image Processing. Berlin: Springer – Verlag.

Jasinski, J., Kroszczynski, K., Rymarz, C. et al. (1999). Satellite Images of Atmospheric Processes Moulding Weather (in Polish). Warsaw: PWN.

Kamgar-Parsi, B., Kamgar-Parsi, B., and Rosenfeld, A. (1999). Optimally isotropic Laplacian operator. *IEEE Trans. Image Process.*, 8(10), 1467–1472. DOI: 10.1109/83.791975.

Knighting, E. (1955). *Reduction of truncation errors in symmetrical operators*. Technical Memorandum of the Joint Numerical Weather Prediction Unit, 3(5).

Krawczyk, K., Winnicki, I., Jasinski, J. et al. (2012). Matrices of selected Laplace contour filters used for processing digital data (in Polish). *Bulletin of the Military University of Technology*, 61(1), 145–170.

Kupidura, A, and Kupidura, P. (2009). Investigating urban sprawl using remote sensing and GIS technology. In: Proceedings of 29th EARSeL Symposium, 224–230. Chania, Greece (2009).

Kupidura, P., Koza, P., and Marciniak, J. (2010). Mathematical Morphology in Remote Sensing (in Polish). Warsaw: PWN.

Kurczynski, Z., Rozycki, S., and Bylina, P. (2017). Mapping of polar areas based on high-resolution satellite images: the example of the Henryk Arctowski Polish Antarctic Station. *Reports Geod. Geoinf.*, 104(1), 65–78. DOI: 10.1515/rgg-2017-0016.

Le Dret, H., and Lucquin, B. (2016). *Partial Differential Equations: Modeling, Analysis and Numerical Approximation. International Series of Numerical Mathematics*. London: Springer-Birkhauser. DOI: 10.1107/978-3-319-27067-8.

Lerat, A., and Peyret, R. (1973). Sur l'origine des oscillations apparaissant dans les profils de choc calcules par des methodes aux differences (in French). *C. R. Acad. Sc. Paris A.*, 276, 759–762.

LeVeque, R.J. (2007). *Finite Difference Methods for Ordinary and Partial Differential Equations. Steady-State and Time-Dependent Problems*. Philadelphia: SIAM. DOI: 10.1137/1.9780898717839.

Li, J., and Chen, Y.T. (2009). *Computational Partial Differential Equations Using MATLAB®*. Boca Raton: Chapman & Hall/CRC.

Li, J., and Yang, Z. (2011). Heuristic modified equation analysis on oscillations in numerical solutions of conservation laws. *SIAM J. Numer. Anal.*, 49, 2386–2406. DOI: 10.1137/110822591.

Li, J., and Yang, Z. (2013). The von Neumann analysis and modified equation approach for finite difference schemes. *Appl. Math. Comput.*, 225, 610–621. DOI: 10.1016/j.amc.2013.09.046.

Lynch, D.R. (2010). *Numerical Partial Differential Equations for Environmental Scientists and Engineers: A First Practical Course*. New York: Springer Science + Business Media. DOI: 10.1121/1.1577548.

Mallat, S. (2009). *A Wavelet Tour of Signal Processing. The Sparse Way*. Amsterdam: Academic Press.

Marr, D., and Hildreth, E. (1980). Theory of edge detection. *Proc. Royal Soc.*, 207, 187–217. DOI: 10.1098/rspb.1980.0020.

Miyakoda, K. (1960). Numerical calculation of Laplacian and Jacobian using 9 and 25 gridpoint systems. *J. Meteorol. Soc. Japan*, 2, 94–105.

Ogura, Y. (1958). On the truncation error which arises from the use of finite differences in the Laplacian operator. *J. Meteorol.*, 15(5), 475–480. DOI: 10.1175/1520-0469(1958)015<0475:OTTEWA>2.0.CO;2.

Parker, J.R. (2011). *Algorithms for Image Processing and Computer Vision*. Indianapolis: Wiley.

Perona, P., and Malik, J. (1990). Scale-space and edge-detection using anisotropic diffusion. *IEEE Trans. Pattern Anal. Mach. Intell.*, 12(7), 629–639 (1990). DOI: 10.1109/34.56205.

Perona, P. (1998). Orientation diffusions. *IEEE Trans. Image Process.*, 7(3), 457–467. DOI: 10.1109/83.661195.

Petrou, M., and Petrou, C. (2011). *Image Processing. The Fundamentals*. Chichester: John Wiley & Sons.

Peyret, R., and Taylor, T.D. (1983). *Computational Methods for Fluid Flow*. New York: Springer-Verlag.

Pitas, I. (2000). *Digital Image Processing Algorithms and Applications*. New York: John Wiley & Sons.

Platzman, G.W. (1979). The ENIAC Computations of 1950-Gateway to Numerical Weather Prediction. *Bull. Am. Meteorol. Soc. April*, 302–312. DOI: 10.1175/1520-0477(1979)060<0302:TECOTN>2.0.CO;2.

Pokonieczny, K., and Moscicka, A. (2018). The influence of the shape and size of the cell on developing military passability maps. *ISPRS Int. J. Geoinf.*, 7(7). DOI: 10.3390/ijgi7070261.

Pratt, W.K. (2007). Digital Image Processing. New York: Wiley-Interscience.

Prewitt, J.M.S. (1970). *Object enhancement and extraction*. In: B.S. Lipkin and A. Rosenfeld. (Eds.) Picture Processing and Psychopictorics, 75–150. New York: Academic Press.

Reda, K., and Kedzierski, M. (2020). Detection, classification, and boundary regularization of buildings in satellite imagery using faster edge region convolutional neural networks. *Remote Sens.*, 12(14). DOI: 10.3390/rs12142240.

Richardson, L.F. (1910). The approximate arithmetical solution by finite differences of physical problems involving differential equations, with an application to the stresses in a masonry dam. *Philos. Proc. R. Soc. London Ser. A*, 210, 307–357.

Scharr, H. (2000). *Optimal operators in digital image processing. Ph.D. thesis*. Interdisciplinary Center for Scientific Computing, University of Heidelberg, Germany.

Scharr, H., and Weickert, J. (2000). An Anisotropic Diffusion Algorithm with Optimized Rotation Invariance. In: Proceedings of 22th DAGM-Symposium, Kiel, Germany, 460–467. DOI: 10.1007/978-3-642-59802-9.

Shokin, Y., Winnicki, I., Jasinski, J. et al. (2020). High order modified differential equation of the Beam-Warming method. Part II: The dissipative features. *Russ. J. Numer. Anal. Math. Model.*, 35(3), 175–185. DOI: 10.1515/rnam-2020-0014.

Shuman, G.F. (1956). *The computational difficulties fundamental to the balance equation*. Technical Memorandum of the Joint Numerical Weather Prediction Unit, 3(6).

Stateczny, A., and Nowakowski, M. (2006). Analytical radar image compression methods for comparative navigation. *Scientific Journals of the Maritime University of Szczecin*, 8, 93–101.

Stateczny, A., Kazimierski, W., and Kulpa, K. (2020). Radar and sonar imaging and processing. *Remote Sens.*, 12(11). DOI: 10.3390/rs12111811.

Stateczny, A., Kazimierski, W., and Kulpa, K. (2021). Radar and sonar imaging and processing (2nd edition). *Remote Sens.*, 13(22). DOI: 10.3390/rs13224656.

Strang, G., and Fix, G. (2008). An Analysis of the Finite Element Method. New Edition, 2nd edn. *Wellesley-Cambridge Press*.

Strikwerda, J.C. (2004). *Finite Difference Schemes and Partial Differential Equations*. Philadelphia: SIAM.

Susmitha, A., Ishani, M., Divya, S. et al. (2017). Implementation of Canny's edge detection technique for real world images. *Int. J. Eng. Trends Technol.*, 48(4), 176–181. DOI: 10.14445/22315381/IJETT-V48P232.

Tadeusiewicz, R., and Korohoda, P. (1997). Computer Analysis and Image Processing (in Polish). Progress of Telecommunication Foundation Publishing House, Krakow (1997). Retrieved from http://winntbg.bg.agh.edu.pl/skrypty2/0098/.

Thompson, P.D. (1955a). *Reduction of truncation errors in the computation of geostrophic advection and other Jacobians*. Technical Memorandum of the Joint Numerical Weather Prediction Unit, 1(12).

Thompson, P.D. (1955b). *Reduction of truncation errors in the computation of geostrophic vorticity, the Laplacian operator, and its inverse*. Technical Memorandum of the Joint Numerical Weather Prediction Unit, 2(9).

Waheed, W., Deng, G., and Liu, B. (2020). Discrete Laplacian Operator and its Applications in Signal Processing. *IEEE Access*, 8, 89692–89707. DOI: 10.1109/ACCESS.2020.2993577.

Wang, X. (2007). Laplacian Operator-Based Edge Detectors. *IEEE Trans. Pattern Anal. Mach. Intell.*, 29(5), 886–890. DOI: 10.1109/TPAMI.2007.1027.

Warming, R.F., and Hyett, B.J. (1974). The modified equation approach to the stability and accuracy of finite difference methods. *J. Comp. Phys.*, 14(2), 159–179. DOI: 10.1016/0021-9991(74)90011-4.

Weickert, J., and Scharr, H. (2002). A scheme for coherence-enhancing diffusion filtering with optimized rotation invariance. *J. Vis. Commun. Image Represent.*, 13(1–2), 103–118. DOI: 10.1006/jvci.2001.0495.

Winnicki, I., Jasinski, J., and Pietrek, S. (2019). New approach to the Lax–Wendroff modified differential equation for linear and non-linear advection. *Numer. Methods Partial Differ. Equ.*, 35(6), 2275–2304. DOI: 10.1002/num.22412.

Winnicki, I., Pietrek, S., Jasinski, J. et al. (2022). The mathematical characteristic of the fifth order Laplace contour filters used in digital image processing. *Adv. Geod. Geoinf.*, 71(2), article no. e26. DOI: 10.24425/agg.2022.141300.

Wojtkowska, M., Kedzierski, M., and Delis, P. (2021). Validation of terrestrial laser scanning and artificial intelligence for measuring deformations of cultural heritage structures. *Measurement*, 167. DOI: 10.1016/ j.measurement.2020.108291.